# Black carbon variability since preindustrial times in Eastern part of Europe reconstructed from Mt Elbrus, Caucasus ice cores

Saehee Lim[1, *], Xavier Faïn[1], Patrick Ginot[1, 2], Vladimir Mikhalenko[3], Stanislav Kutuzov[3], Jean-Daniel Paris[4], Anna Kozachek[3] and Paolo Laj[1, 2]

1 Univ. Grenoble-Alpes, CNRS, Institut des Géosciences de l'Environnement, Grenoble, France.

2 Univ. Grenoble-Alpes, CNRS, IRD, Observatoire des Sciences de l'Univers, Grenoble, France.

3 Institute of Geography, Russian Academy of Sciences, Moscow, Russia.

4 Laboratoire des Sciences du Climat et de l'Environnement, IPSL, CEA-CNRS-UVSQ, CE Orme des Merisiers, 91190 Gif sur Yvette, France.

*now at: Department of Earth and Environmental Sciences, Korea University, Seoul, South Korea.

*Corresponding to*: S. Lim (saehee.lim@gmail.com)

**Abstract** Black carbon (BC), emitted by fossil fuel combustion and biomass burning, is the second largest man-made contributor to global warming after carbon dioxide (Bond et al., 2013). However, limited information exists on its past emissions and atmospheric variability. In this study, we present the first high-resolution record of refractory BC (rBC, including mass concentration and size) reconstructed from ice cores drilled at a high-altitude Eastern European site in Mt. Elbrus (ELB), Caucasus (5115 m a.s.l.). The ELB ice core record, covering the period 1825-2013, reflects the atmospheric load of rBC particles at the ELB site transported from the European continent with a larger rBC input from sources located in the Eastern part of Europe. In the first half of the 20th century, European anthropogenic emissions resulted in a 1.5-fold increase in the ice core rBC mass concentrations as respect to its level in the preindustrial era (before 1850). The summer (winter) rBC mass concentrations increased by a 5-fold (3.3-fold) in 1960-1980, followed by a decrease until ~2000. Over the last decade, the rBC signal for summer time slightly increased. We have compared the signal with the atmospheric BC load simulated using past BC emissions (ACCMIP and MACCity inventories) and taken into account the contribution of different geographical region to rBC distribution and deposition at the ELB site. Interestingly, the observed rBC variability in the ELB ice core record since the 1960s is not in perfect agreement with the simulated atmospheric BC load. Similar features between the ice core rBC record and the best scenarios for the atmospheric BC load support that anthropogenic BC increase in the 20th century is reflected in the ELB ice core record. However, the peak in BC mass concentration observed in ~1970 in the ice core is estimated to occur a decade later from past inventories. BC emission inventories for the period 1960s-1970s may be underestimating European anthropogenic emissions. Furthermore, for summer time snow layers of the last 2000s, the slightly increasing trend of rBC deposition likely reflects recent changes in anthropogenic and biomass burning BC emissions in the Eastern part of Europe. Our study highlights that the past changes in BC emissions of Eastern Europe need to be considered in assessing on-going air quality regulation.

## 1 Introduction

Climate forcing of black carbon (BC), a primary aerosol emitted by fossil fuel and biomass combustions, is of

great concern due to its strong light-absorbing ability and small size allowing it to be transport over long distances (Bond et al., 2013; Ramanathan and Carmichael, 2008). In high-altitude or high–latitude areas, BC has been identified as a significant contributor in accelerating snowmelt (Hansen and Nazarenko, 2004; Xu et al., 2016). Despite numerous studies through both measurements and model simulations (Bond et al., 2013 and references therein), little is known about BC's past variability, e.g., before year 2000, and sensitivity to climate change primarily due to limited in-situ atmospheric BC measurements both temporally and spatially (Collaud Coen et al., 2007, 2013).

Reconstruction of atmospheric BC variability from ice core archives can thereby be very helpful to understand past BC emissions and provide additional constraint on BC emission inventories (Bisiaux et al., 2012a; Kaspari et al., 2011; Legrand et al., 2007; McConnell et al., 2007; Wang et al., 2015). Particularly, the geographical proximity of the ice cores at high-altitude Alpine sites, e.g., European Alpine sites such as Col du Dôme, Colle Gnifetti and Fiescherhorn (Jenk et al., 2006; Legrand et al., 2013; Thevenon et al., 2009) to densely populated regions (approximately ~100 km) allows us to observe a fingerprint of BC emissions and past temporal variability in the anthropogenic source regions. In this respect, elemental carbon (EC) records reconstructed from ice cores at Western European Alpine sites (Col du Dôme and Colle Gnifetti) highlight a pronounced EC increase starting mid-20th century (Legrand et al., 2007; Thevenon et al., 2009) with increasing anthropogenic activity in the Western Europe (Fagerli et al., 2007; Lamarque et al., 2010). It should be noted that EC refers to data derived from thermal methods which are different than optical methods providing BC (including rBC derived from incandescence methods) (Petzold et al., 2013). However, recent EC records over the last two decades are not available from these Western European ice cores, which makes it difficult to quantify historic BC emissions and thus provide implications for assessing European air quality regulation initiated since 1970 (Tørseth et al., 2012; Vestreng et al., 2007). Furthermore, long-term ice core BC records have never been reconstructed from the Eastern European regions where even atmospheric measurements are relatively scarce (Pio et al., 2007; Yttri et al., 2007). Reconstruction of BC records with a wide range of coverage both temporally and spatially is crucial to understand BC emission properties and establish regulations on the emissions.

In this study, we present a high-resolution record of refractory BC (rBC) deposition to snow at a high-altitude site in Mt. Elbrus, Caucasus (5115 m a.s.l.) covering the period 1825-2013. Located between the Black and the Caspian seas, Mt. Elbrus is influenced by prevailing westerly from the European continent (Mikhalenko et al., 2015). For the first time, a high resolution, continuous rBC record was extracted from an ice core over Europe. The Elbrus rBC record thus brings new and unique information on long-term variability and evolution of BC European emissions. The study documents the variability of rBC deposition and provides a comparison with the expected atmospheric BC variability based on past emission inventories also considering atmospheric transport to the drilling site.


## 2. Method

### 2.1 Ice core drilling site

A 181.8 m-long ice core (the 2009 core) was drilled at the Western Plateau of Mt. Elbrus (ELB), the highest summit of the Caucasus (43°20'53,9"N, 42°25'36,0"E, 5115 m a.s.l.) (Figure 1) on September 2009. In addition, a 20.5 m-long ice core (the 2013 core) was extracted in June 2013 at the same site to expand the existing ice-core

76　sample set from 2009 to 2013. Drilling was performed in a dry borehole with a lightweight electromechanical

77　drilling system, and was accompanied by borehole temperature measurements. Borehole temperatures ranged

78　from -17 °C to 10 m depth to -2.4 °C at 181 m of the 2009 core (Mikhalenko et al., 2015).

79　The core were packed in polyethylene sealed bag and stored on the glacier at -10°C. After the drilling campaign,

80　the core were packed in insulated core boxes and shipped frozen to the cold laboratory of the Lomonosov

81　Moscow State University for preliminary investigation and water stables isotopes analyzes. In Moscow, the core

82　was split and one-half was shipped to LGGE (Laboratoire de Glaciologie et Géophysique de l'Environnement -

83　now Institut de Géophysique de l'Environnement) in Grenoble, France for additional analyzes.

84

85　**2.2 rBC ice core analysis**

86　The top 156.6 m of the 2009 core and the entire 2013 core were analyzed at LGGE in 2013-2014 and in 2014,

87　respectively, using an ice core melter system coupled with a jet nebulizer (APEX-Q, Elemental Scientific Inc.,

88　Omaha, NE) and a single particle soot photometer (SP2, Droplet Measurement Technologies, Boulder,

89　Colorado). We have used the terminology proposed by Petzold et al. (2013) for incandescence-based BC

90　measurements. Our results are therefore reported in terms of refractory-BC (rBC). It should be noted that there is

91　a direct relationship (although not necessarily linear) between rBC and BC measured with other techniques

92　(Kondo et al., 2011a; Laborde et al., 2012; Miyakawa et al., 2016).

93　Dust and conductivity are continuously analyzed simultaneously to rBC. Briefly, ice core sticks (3.4 cm x 3.4 cm

94　x 1 m) were melted at a mean rate of 3 cm min$^{-1}$ and the melt water from the inner 6.8 cm$^2$ of the sticks were

95　continuously collected. After de-bubbling, the sample flow was split to rBC analytical line with a mean flow of

96　about 70±10 μL min$^{-1}$. The flow rate dedicated to rBC analyses was continuously recorded using a mass flow

97　meter (SENSIRION© SLI-2000). In parallel, the melt water was sampled by two auto-samplers at the end of the

98　CFA for off-line ionic species analysis and archive storage. The upper section of the 2009 firn core (surface to

99　7.2 m depth) was analyzed discretely.

100　 Ice core rBC analysis using the SP2 has been reported previously (Bisiaux et al., 2012a, 2012b; Ginot et al.,

101　2014; Jenkins et al., 2013; Kaspari et al., 2014; Wang et al., 2015). Specifically, recent papers describe detailed

102　analytical evaluation for rBC in liquid samples, e.g., rain, snow and ice core, using the SP2 (Lim et al., 2014;

103　Mori et al., 2016; Schwarz et al., 2012; Wendl et al., 2014). The SP2 uses a laser-induced incandescence method

104　to measure the mass of individual rBC particle (Schwarz et al., 2006; Stephens et al., 2003). Briefly, an

105　individual rBC particle passes through the laser beam intra-cavity of a 1,064 nm Nd:YAG laser and

106　incandescences. Of two PMT-photo detectors (broad and narrow bands) that are used to detect incandescence

107　signal, we used only broadband detector to derive rBC mass avoiding low signal-to-noise ratio from the

108　narrowband detector. The SP2 was calibrated by analyzing mass-selected fullerene soot (Alfa Aesar Inc., USA).

109　The design and gain settings of our SP2 resulted in the lower and upper limit of measurements for rBC mass to

110　be ~0.3-220 fg. A particle larger than 220 fg was treated as the particle of 220 fg. Loss of rBC particles occurring

111　during aerosolization in the APEX-Q was calibrated and corrected daily by rBC standard solutions (Aquadag®,

112　Acheson Inc., USA; 8 steps from 0.1 to 100 μg L$^{-1}$), which resulted in rBC mass recovery of 75±7 %. The rBC

113　fraction that was not aerosolized was partially identified in drains and internal surface of the APEX-Q (see

114　Supplementary information in Lim et al. (2014)). To prevent contamination and achieve the rBC levels as low as

possible, both an instrumental blank (ultrapure water) and a 5-cm procedure blank (frozen ultrapure water cut in the cold room) were run daily prior to field sample analysis, until the rBC counting reached 0 to 1 per second, equivalent to rBC concentration of less than 0.01 µg L$^{-1}$.

High resolution continuous rBC data recorded every second was smoothed at a depth resolution of 1 cm, except the upper section (surface to 7.2 m depth) of the 2009 core that was discretely analyzed at a depth resolution of ~5-10 cm. The density of rBC data points per year (N=8~376) depends on annual snow accumulation rates and ice thinning with depth. The two ice cores are overlap for snow layers of year 2007-2009 (Fig. S1). The records described here for rBC concentrations are (i) the 2009 ice core from 2.9 m to 156.6 m, corresponding to calendar years of 1825-2008 and (ii) the top 15.9 m of the 2013 core, corresponding to calendar years of 2009-2013. These two ice core records cover the calendar years of 1825-2013.

As a first survey for long-term rBC size distributions of ice core record, mass equivalent diameter of measured single rBC particle, $D_{rBC}$, was calculated, assuming a void-free BC density of 1.8 g cm$^{-3}$ (Moteki and Kondo, 2010). The calculated $D_{rBC}$ was in the range of ~70 and 620 nm. A series of test using mono-dispersed polystyrene latex (PSL) spheres with known diameters (150-600 nm) and poly-dispersed standard BC (Aquadag®) suggests that the APEX-Q/SP2 system preserves original size information of rBC particles in liquid samples and provides highly reproducible rBC size measurements with a variation of < 5 nm (Sect. 2.2.3 and 2.2.5 in Lim et al., 2014; Wendl et al., 2014). rBC size distributions were retrieved seasonally and simplified with a log-normal fit with a bin size (#)=200. Mass mode diameter (MMD) of the log-normal fit was then extracted to further reduce parameters. Size intervals between bin channels vary, with the minimum interval of less than 8 nm for the MMD 200-350 nm. Here, all SP2 data were processed with the SP2 toolkit developed by M. Gysel at the Paul Scherrer Institute (PSI, Switzerland; http://aerosolsoftware.web.psi.ch/).


**2.3 Ice core dating and seasonal signature**

Ice core dating was determined by counting annual layers from 1825 to 2013 using the seasonal cycles of ammonium (NH$_4^+$), succinic acid and water stable isotopes (δD and δ$^{18}$O) that were analyzed discretely. Based on the examination of the ammonium and succinic acid profiles, each annual layer was divided into two parts corresponding to snow deposition under winter condition and summer condition (Legrand et al., 2013; Mikhalenko et al., 2015; Preunkert et al., 2000). In addition, the annual layer counting was further confirmed using the reference horizon from a tritium peak (1963) and a volcanic horizon (Katmai in 1912). The mean annual net accumulation rate of 1455 mm w.e. for the last 140 years was estimated from these proxies. The dating uncertainty is 2-year between the top and 106.7 m (Kozachek et al., 2016; Mikhalenko et al., 2015) and probably larger below 106.7 m due to ice thinning. Further details about dating are found in Mikhalenko et al. (2015).

Ice core seasonality was determined by the ammonium stratigraphy and further verified by the isotope variations. However, seasonal separation of the high-resolution rBC record made by lower-resolution ammonium profile was sometimes challenging particularly at the edge of two seasons, misleading winter (summer) rBC layers to be more concentrated (less concentrated) by the adjacent seasonal rBC layer. To avoid inaccurate separation of an annual ice layer into winter and summer intervals, only mid-summer and mid-winter rBC concentrations were extracted by considering data comprised between the 25$^{th}$ percentile and the 75$^{th}$ percentile of the depth thickness

4

154     of each seasonal snow layer. This seasonal separation method is fairly supported by the fact that (i) observed

155     precipitation in the Western Caucasus is equally distributed throughout a year (e.g., at Klukhorskiy Pereval

156     station located 2037 m a.s.l., 50 km westward from the drilling site: 52% of the annual precipitation (resp. 48%)

157     is observed during summer (resp. winter) and each monthly precipitation accounts for 6-11 % of total

158     precipitation for the period 1966-2009; www.meteo.ru) and (ii) maximum or minimum values of both $\delta^{18}O$ and

159     ammonium coincide for most of the Elbrus core annual ice layers. The mid-summer and mid-winter are therefore

160     corresponding roughly to the warmest three months and the coldest three months ("background winter") of a

161     year. Later in the manuscript, summer and winter of this study will refer to mid-summer and mid-winter,

162     respectively.

163

## 2.4 Atmospheric transport modeling

### 2.4.1 Model description and runs

166     FLEXPART v6.2 lagrangian particle dispersion model (LPDM) calculates the trajectories of tracer particles

167     using the mean winds interpolated from the gridded analysis field and parameterizations representing turbulence

168     and convective transport (Forster et al., 2007; Stohl and Thomson, 1999). FLEXPART was run using reanalysis

169     fields of the European Centre for Medium-Range Weather Forecasts (ECMWF, ERA-Interim) at 0.75°×0.75°

170     resolution, which is available since 1979. Here, a backward simulation mode was used to analyze particles

171     transport pathways from potential flux regions to the sampling site (Seibert and Frank, 2004; Stohl et al., 2005).

172     To limit computational cost, simulations were performed for two selected periods: 2005-2009 and 1979-1983.

173     We selected these periods because: (i) year 1979 is the first year of ECMWF data and year 2009 is the last year

174     of our longer ice core (2009 ice core) that were analyzed prior to the 2013 ice core and (ii) these years are

175     inflections in rBC trends (Sect. 3.2). It would thus be sufficient to analyze transport patterns influencing rBC at

176     ELB and determine potential changes in these transport patterns. 1,000 particles are released at the drilling site

177     during every 5-day interval in June to August (JJA) and in December to February (DJF). Modelled global

178     average atmospheric lifetimes of BC particles varies by a factor of more than 3, ranging from 3 to 10 days (Bond

179     et al., 2013). Because BC particles reaching the high-altitude ELB site would experience longer lifetimes than

180     the particles transporting in the planetary boundary layer (PBL), simulations were performed using a BC lifetime

181     of 5-, and 7-day. However, 7-day air mass trajectories were extending to the Pacific and therefore made little

182     difference with the 5 days simulations. Thus we set the BC lifetime as 5-day. Number of particles were then

183     computed every 3h at 0.5°×0.5° resolution.

184

### 2.4.2 Sensitivity by potential source regions

186     The finally defined footprint density $F$ ($i$, $j$, $n$) is expressed as a parameter encompassing released particle

187     number and residence time along the particles pathway, in procedure defined unit (p.d.u.). This final result is

188     theoretically identical to potential emission sensitivity (PES), called source-receptor-relationship by Seibert and

189     Frank (2004), which is proportional to the particle residence time in a particular grid cell with a fixed altitude

190     range.

191     To facilitate analysis we reduced the number of variables from the gridded footprint density by summing them

over large regions. We classified the footprint areas into five geographical regions with specific rBC emission sources (Figure 2). The regions identified are as follows: **EEU** (Eastern Europe including nearby the Mt. Elbrus, Ukraine and Europe Russia and a part of Middle East), **CEU** (Central Europe), **WEU** (Western Europe), **NAF** (North Africa), **NAM** (North America) **and Others** (The Atlantic and a part of Northern Europe above 60°N).

To display our results, we first calculate the footprint density $F$e of the entire footprint area:

$$F\mathrm{e}\,(i,j) = \sum_{\mathrm{n}=1}^{N} F(i,j,n)$$

Here, $F$ ($i$, $j$, $n$) is footprint density, where $i$ and $j$ are the indices of the latitude/longitude grid and $n$ runs over the total number of cases N. $F$e indicates the entire footprint area where the aerosols track during the last 5 days of transport. Note that we found little inter-annual variability in the footprint contribution of each region to the ELB site with a 3 % variation over the two periods (2005-2009 and 1979-1983). Assuming that this inter-annual variability in footprint density is not large enough to influence on long-term rBC trends and the results over the two periods are thus fairly representative of 20th century, we combined the simulations results and used this approach to study long-term emission contribution of each geographical region to rBC distribution and deposition at our drilling site.

In addition to the calculation using total particles in the atmospheric column, calculations using particles positioned in the lowest 2 km layers in the atmosphere were performed to investigate emission source regions of aerosols transporting from low altitudes, while the simulation procedure is the same as for the entire atmospheric column. To show the potential particle transport strength of each region relative to the entire area, we calculated the percentages of the footprint density in each region relative to the one in the entire area. To do this, we sum $F$e ($i$, $j$) over the entire footprint area resulting in one value. In the same way, we sum $F$ ($i$, $j$) within each of the five regions resulting in five values.

## 2.5 Historic BC emission inventories

To describe temporal variability in the regional BC emissions and atmospheric load of BC transported to the ELB site, we used time-varying anthropogenic and biomass burning BC emissions estimated by ACCMIP (Emissions for Atmospheric Chemistry and Climate Model Intercomparison Project) inventory for the period 1900-2000 on the decadal scale (at 0. 5°×0. 5° resolution; Lamarque et al., 2010) and MACCity (MACC/CityZEN EU projects) inventory for the year 2008 (at 0. 5°×0. 5° resolution; Diehl et al., 2012; Granier et al., 2011; Lamarque et al., 2010; van der Werf et al., 2006). Note that the ACCMIP inventory provide decadal means (e.g., '1980' corresponds to the mean of 1980-1989) for the biomass burning estimates and representative values (e.g., '1980' is a representative of 1975-1985) for the anthropogenic estimates, leading to 5-year shift between two estimates. We used anthropogenic emission only for constraining BC emissions in DJF and both anthropogenic and biomass burning emissions for constraining BC emissions in JJA, because seasonal biomass burning BC emissions are maximized in summer time (May to August), being two orders of magnitude larger than during winter time (September to February), as respect to anthropogenic emissions occurring year-round (Lamarque et al., 2010).

**3 Results and discussion**

**3.1 High resolution rBC record from Elbrus ice cores**

We present the first high-resolution rBC record of ice cores drilled in the Mt. Elbrus, Caucasus (2009 and 2013 cores, Figure 3a). The rBC concentrations along the two cores ranged from 0.01 μg L$^{-1}$ to 222.2 μg L$^{-1}$ with a mean±1σ of 11.0±11.3 μg L$^{-1}$ and a median of 7.2 μg L$^{-1}$. A 20-m long section is zoomed in Figure 3b to highlight the higher resolution of rBC signals when continuously recorded at 1-cm depth interval compared to the surface snow and firn section (from top to 7.2 m) analyzed discretely at ~5-10 cm-depth interval. The rBC record was found to preserve sub-annual variability from top to depth of 156.6 m with rBC spikes reflecting large and abrupt variability in deposition of atmospheric rBC particles. Such high-resolution record brings new opportunities to study dynamic atmospheric vertical transport and/or sporadic events in a season.

A well-marked seasonal rBC cycle (e.g., Fig 3b) was characterized for the 2013 core and the 2009 core down to 156.6 m by consistent high summer values ranging from 0.2 to 222.2 μg L$^{-1}$ with a mean±1σ of 15.5±12.9 μg L$^{-1}$ and a median of 11.7 μg L$^{-1}$ and low winter values ranging from 0.2 to 44.6 μg L$^{-1}$ with a mean±1σ of 5.9±5.1 μg L$^{-1}$ and a median of 4.5 μg L$^{-1}$ (Table 1). The highest rBC mass concentration of an annual snow layer was observed in summer snow layer. In atmospheric observations at ground-based sites in Western and Central Europe boundary layer, EC aerosol mass concentrations in winter are higher roughly by a factor of 2 than in summer mainly due to the enhanced domestic heating (Pio et al., 2007; Tsyro et al., 2007). In contrast to the boundary layer sites, the atmospheric measurements at high-elevation sites in Europe (e.g., Puy de Dôme at 1465 m a.s.l., Sonnblick at 3106 m a.s.l. and Jungfraujoch at 3580 m a.s.l.) revealed 2 to 3 times higher EC levels during summer than winter (Bukowiecki et al., 2016; Pio et al., 2007; Venzac et al., 2009), reflecting the efficient upward transport of BC aerosols from the polluted boundary layer to the high-altitudes during summer, primarily by thermally-driven convection and thickening boundary-layer height (Lugauer et al., 1998; Matthias and Bösenberg, 2002). This is consistent with the rBC seasonality observed in the ELB ice core.


**3.2 Long term evolution of rBC mass concentrations**

Time series of seasonal (summer and winter) and annual medians of rBC mass concentrations from 1825 to 2013 are shown in Figure 4. Medians are shown with lower and upper 10$^{th}$ percentiles to illustrate rBC concentrations. The rBC concentrations varied significantly over the past ~190 years with a large inter-annual variability. Summer, winter and annual rBC medians increased gradually since the onset of 20$^{th}$ century with a rapid increase in ~1950 lasting until ~1980. 10-year moving averaged rBC values reached their maximums in the 1960s and 1970s.

Concentrations and relative change to levels of preindustrial era (here, defined as 1825-1850) for given time periods are summarized in Table 1. For the period of 1825-1850, median (± standard deviation, SD) of rBC concentrations were 4.3±1.5 μg L$^{-1}$ in summer and 2.0±0.9 μg L$^{-1}$ in winter. The rBC concentrations increased by a ~1.5-fold in 1900-1950. Meanwhile, the slight increase of winter rBC values in 1900-1920 with respect to summer rBC values are not well understood. Although speculative, it may reflect increased winter BC inputs transporting through the free troposphere (FT) from North America, where BC emissions markedly increased at the beginning of 20$^{th}$ century (Lamarque et al., 2010; McConnell et al., 2007). Over the period of 1960-1980,

268  rBC concentrations increased by a factor of 5.0 in summer and a factor of 3.3 in winter. The larger relative
269  change of summer rBC than one of winter for the period suggests that rBC emissions in summer source region
270  increased more sharply for this time period. Notably, in addition to medians, the lower $10^{th}$ percentiles of both
271  summer and winter rBC increased since the preindustrial era, highlighting that rBC background level in the
272  atmosphere at ELB was also significantly modified. Meanwhile, upper $10^{th}$ percentiles ranged up to 75 µg $L^{-1}$, 35
273  µg $L^{-1}$ and 56 µg $L^{-1}$ for summer, winter and annual variability, respectively.

274  Of the EC records available in the Western European mountain glaciers, only Col du Dôme (hereafter, CDD;
275  Legrand et al., 2007) and Colle Gnifetti (hereafter, CG; Thevenon et al., 2009) summer records provide EC
276  records for the recent time (until ~1990 and 1980, respectively), whereas the Fiescherhorn (hereafter, FH; Jenk et
277  al., 2006) record is available until 1940 only. Both summer records at CDD and CG show somewhat comparable
278  preindustrial EC levels (~2 µg $L^{-1}$ for CDD and ~7 µg $L^{-1}$ for CG in the mid-1800s) to the ELB rBC (4.3±1.5 µg
279  $L^{-1}$ in 1825-1850) and substantially increased EC concentrations for the period 1950-1980 since the mid-$19^{th}$
280  century, similar to the ELB rBC. This suggests that EC emissions show a common trend at the European scale,
281  and that such trend has been recorded in the different European high-altitude ice cores from CDD, CG, and ELB.
282  Some differences, such as peak time period and increase/decrease rate between records that may reflect sub-
283  regional (e.g., Western Europe vs. Eastern Europe) emission changes, may be also noteworthy. However, direct
284  comparison of the ELB rBC with the Western European ice core records should be made with caution owing to
285  both (i) different analytical methods applied for the ice cores (e.g., ELB rBC: APEX-Q/SP2, CDD EC: thermal-
286  optical method with EUSAAR2 protocol, and CG EC: thermal method) (Lim et al., 2014) and (ii) lower data
287  resolution particularly for the CDD core (a few data points for a decadal EC concentration).  We thus focus on
288  evaluating the ELB rBC record in Sect. 3.5 by comparing with simulated atmospheric load of BC particles that
289  were transported from source regions to the Mt. Elbrus.
290

### 3.3 Past variability in rBC size distributions

292  The first record of temporal and seasonal changes in rBC size distribution was extracted from the ELB ice core.
293  Mass equivalent diameter of rBC particles ($D_{rBC}$) was log-normally distributed. The mode of rBC mass size
294  distributions (mass mode diameter, MMD) was determined for both summer and winter layers by fitting a log-
295  normal curve to the measured distribution (e.g., Figure S2). This approach provides reliable results of
296  representative rBC size in seasonal ice layers as the determined MMDs fall into the measured size range (~70-
297  620 nm).
298  Figure 5 shows time series of rBC MMD for the period of 1940 to 2009. The upper and lower limits of the
299  periods selected for retrieving rBC MMD were chosen so as a large number of rBC particles in the seasonal ice
300  layer would be available and would allow to secure reliable size distribution of the ice layer. Faster melting of
301  snow layers of year 2010-2013 and thinner ice layers below the layer of year 1940 did not allow to record
302  sufficient numbers of rBC particles and thus robust rBC size distributions could not be retrieve. For the
303  considered time period, rBC MMD of both summer and winter layers varied ranging from 207.3 nm to 378.3 nm
304  with a geometric mean of 279.4±1.1 nm. No statistically significant temporal change in rBC MMD was
305  identified over the 1940-2009 period.
306  Notably, rBC particles measured in this study show the MMD shifted to larger sizes than those measured in the

atmosphere over Europe (MMD of 130-260 nm) (Dahlkötter et al., 2014; Laborde et al., 2013; Liu et al., 2010; McMeeking et al., 2010; Reddington et al., 2013), even larger than atmospheric rBC diameter measured at an high alpine site, Jungfraujoch (JFJ) in Switzerland (MMD of 220-240 nm) (Liu et al., 2010). The shift of rBC sizes induced by dry deposition should be negligible, as quite high (100-200 mm/month) and fairly constant precipitation rate throughout the year near the drilling site (e.g., 52 % and 48 % of annual precipitation observed in summer and winter, respectively, at Klukhorskiy Pereval station (see Sect. 2.3)) suggests that wet deposition can be the dominant aerosol removal pathway at this site. Similarly, significant snow melt was not observed in the ELB summer ice layers. Although there is a lack of studies about the impact of snow melting on rBC size distribution, such processes would not be expected at the ELB drilling site. Rather, the different rBC size distributions of the ice core from those in the atmosphere are likely associated with removal process of rBC particles during precipitation. Recent study using the SP2 technique showed the rBC size distribution in rainwater shifted to larger sizes (MMD= ~200 nm) than that in air (MMD= ~150 nm) in Tokyo, indicating that large rBC particles were more efficiently removed by precipitation (Mori et al., 2016). The preferential wet removal of larger rBC particles (Mori et al., 2016; Moteki et al., 2012) could reasonably explain the larger MMD of rBC particles observed in the ice core than atmospheric rBC aerosols (Schwarz et al., 2013).

The difference in seasonal rBC size distributions was statistically significant ($p<0.01$). In summer, the MMD varied ranging from 227.4 nm to 378.3 nm with a geometric mean of 290.8±1.1 nm (Fig.5, red curve). In winter, the MMD varied ranging from 207.3 nm to 344.9 nm with a geometric mean of 268.7±1.1 nm (Fig.5, blue curve). The rBC MMD of summer ice layers tended to be slightly larger than that of winter layers. Despite few observational evidences, we hypothesize that larger rBC size in summer may reflect advection of rBC aerosols transported from the PBL by thermally-driven convection, while in winter aerosols transported in the FT could be smaller due to longer residence time in the atmosphere and accordingly, more chances for larger aerosols to be removed by precipitation prior to reaching the ELB site. Our hypothesis seems to be reasonable being consistent to the findings of in-situ aerosol measurements at high-altitude sites in Europe. Liu et al. (2010) found that rBC aerosols at JFJ were slightly larger when the site was influenced by valley sources, anthropogenic pollutants from lower altitudes. Submicron aerosol size distributions were also overall shifted to larger size in summer (50 to 150 nm) than in winter (below 50 nm) at European mountain stations with altitude of ~1000-3000 m a.s.l. (Asmi et al., 2011). The authors in the latter explained this feature by relatively polluted air masses from the PBL during daytime in summer, but more influence of the FT air masses in winter. Similar to the clear seasonal cycle in rBC mass concentration, the clear seasonal rBC size distributions of the ELB ice core point out seasonal differences in origins of air masses reaching the ELB drilling site: PBL air with less chance of aerosol wet removal in summer and the free tropospheric air in winter.

In addition, the larger rBC MMD in summer layers can be associated with specific summer sources of atmospheric rBC particles, such as forest fires and/or agricultural fires. Particularly, forest fires in Southern Europe and agricultural fires in Eastern Europe may well contribute to summer aerosol loading in Europe (Bovchaliuk et al., 2013; van der Werf et al., 2010; Yoon et al., 2011). Previous SP2 studies have reported the larger size of rBC aerosols for biomass burning plumes, e.g., MMD of ~200 nm (Kondo et al., 2011b; Schwarz et al., 2008; Taylor et al., 2014) compared to rBC sizes for urban plumes. In the ELB ice core, we observed a maximum rBC MMD of 378.3 nm, with a maximum rBC mass concentration of 222.2 μg L$^{-1}$ in the late summer snow layer of year 2003, when extreme forest fire events occurred over the Iberian Peninsula and the

347  Mediterranean coast (Barbosa et al., 2004; Hodzic et al., 2006) resulting from a record-breaking heatwave in

348  Europe (Luterbacher et al., 2004; Schär et al., 2004). Both forward and backward air mass trajectories calculated

349  from HYSPLIT model support that the ELB site was potentially influenced by the intense forest fires occurred in

350  the Southern part of Europe on the mid-August 2003 (Fig. S3), when the top altitude of the PBL was estimated to

351  be ~4.5 km high (Hodzic et al., 2006). Although speculative, this snow layer of year 2003 peaked with rBC

352  concentration and enriched with larger-sizes rBC particles indicates potential contribution of biomass burning

353  aerosols transported westerly to the ELB site. This 2003 summer snow layer experienced some melting

354  (Kozachek et al., 2016), but we can rule out that such melting was driving the unusual MMD signal described

355  above and other snow layers with melting event did not show any anomalies of rBC MMD toward larger values.

356  The rBC size distributions preserved in Elbrus cores could be discussed as an influence of seasonal vertical

357  transport versus emission sources of rBC aerosols and their wet removal properties. This rBC size information is

358  potential to provide important implications particularly for the determination of snow-melting potential by rBC

359  particles in snow (Flanner et al., 2007; Schwarz et al., 2013). Comparison of rBC size with well-established

360  biomass burning proxies would be required to better characterize the dependency of rBC sizes with past fire

361  activities.

362

### 3.4 Potential emission source regions

364  Figure 6 illustrates potential source regions of BC aerosols reaching the ELB site. The model results show that

365  relative to the footprints in JJA, footprints in DJF were more spread out of European continent and extended

366  further over the Pacific (Figure 6a and b). The relative contributions of each regional footprint density over the

367  total density are summarized in Fig. 7. Most of aerosols reaching the ELB site are transported from the European

368  continent (WEU+CEU+EEU) accounting for 71.0 % and 55.6 % in JJA and DJF, respectively and particularly

369  from the Eastern part of Europe (CEU+EEU) accounting for 59.0 % and 47.0 % in JJA and DJF, respectively.

370  The region EEU brings the greatest contribution with fairly consistent features for both seasons, accounting for

371  35.6 % and 30.9 % in JJA and DJF, respectively. A stronger seasonality was found in the region NAF and the

372  region NAM, where the footprint contribution was larger in DJF by a 2-fold. This seasonal variation is caused by

373  longer particle trajectories promoted by a faster zonal flow in winter across the North Atlantic from west to east.

374  To investigate contributions of aerosols transporting from low altitudes which may reflect emissions at surface

375  more sensitively, we calculated the footprint density of particles positioned in the lowest 2 km layers in the

376  atmosphere. Note that we arbitrarily selected this vertical height of atmosphere (2 km layer) since particles

377  positioned at lower atmosphere (e.g., ~1 km layer) was rarely observed in our simulations and the PBL heights

378  were often higher in European mountains up to 3 km (Matthias et al., 2004). The results for JJA show that unlike

379  in the entire atmospheric column, the contribution of footprint density from the region EEU was almost doubled

380  in the 2 km layer, accounting for 63.6 % (Fig. 6c). Contrarily, in DJF, the proportion of the region EEU was only

381  22 % over total footprint density in this fixed layer. We thus infer that large seasonal increases observed during

382  summer time in rBC mass concentration are likely driven by deposition of rBC aerosols transported from Eastern

383  part of Europe and mostly originating from lower altitudes.

384  Therefore, these FLEXPART results confirm that rBC deposition to the Mt. Elbrus is most likely dominated by

385  transport of BC emissions from the European continent, with the strongest BC inputs from the Eastern part of

386     Europe particularly in summer.

387

388     **3.5 New constrains on European BC emissions**

389     Refractory BC concentrations of the ELB ice core increased rapidly from the 1950s to the 1980s (Figure 4 in

390     Sect. 3.2), and such trend record should primarily reflect changes in European BC emissions (Sect. 3.4). Here,

391     we compare past emission BC inventories with the ELB ice core record to bring new constrains on past

392     European BC emissions.

393     Figure 8 shows temporal changes in anthropogenic and biomass burning BC emissions for the period 1900-2008

394     estimated by ACCMIP and MACCity (Diehl et al., 2012; Granier et al., 2011; Lamarque et al., 2010; van der

395     Werf et al., 2006). The overall emission trends (black lines) illustrate a decrease of anthropogenic emissions

396     since 1900 (Figure 8a) and a high variability of biomass burning emissions over the whole period (Figure 8b).

397     For anthropogenic emissions, the largest BC emissions in EEU and CEU regions occurred in 1980, followed by

398     decreasing trends. WEU had the strongest BC emissions lasting until 1960, followed by a decrease of BC

399     emissions lasting the present-day. In 2008, anthropogenic BC emissions in region EEU, CEU and WEU are

400     comparable with an order of 0.2 Tg yr$^{-1}$.

401     To investigate factors controlling long-term rBC trends preserved in the ELB ice core, the temporal evolution of

402     measured ice core rBC particles can be directly compared with that of atmospheric BC load at the ELB site, at

403     least in relative manner. This comparison is provided in Fig. 9, in which ice core record is averaged along a

404     decadal scale to be comparable with the historic BC emission data available on decadal scale only (Lamarque et

405     al., 2010). Specifically, we coupled the BC emission intensities in each region and their relative contribution to

406     the entire footprint area of ELB site (Figure 8c and d). The decadal BC emission burden in each region (Figure

407     8a and b) is therefore multiplied by the contribution of footprint density (Figure 7). Assumption behind this

408     comparison is that (i) the atmospheric circulation and transport patterns do not change with time and (ii) that the

409     mechanisms for BC depositing on snow remained constant. Hence, the proportionality between BC mass

410     concentration in snow and atmospheric BC load has not varied with time.

411     For summertime (JJA case, Fig. 9a) optimal agreement in trend pattern is observed between the ice core rBC

412     and the atmospheric BC estimated in the lower 2 km layer with an increase at the onset of the 20$^{th}$ century and a

413     subsequent decrease since ~1980 ("best scenario"). Specifically, substantial increase in atmospheric BC load is

414     observed for the period 1910-1970, similar to the ELB rBC ice core record, only when the atmospheric BC

415     considers BC particles transported in the lowest 2 km layer of the atmosphere. On the other side, the estimation

416     derived from the entire atmospheric column does exhibit a different pattern. This comparison indicates that

417     changes primarily in European anthropogenic BC emissions (e.g., industry, traffic and residential combustion),

418     particularly ones of Eastern part of Europe, are consequently reflected in the ELB ice core rBC variability over

419     the last century.

420     For wintertime (DJF case, Fig. 9b), the ice core rBC variability before 1980 can be explained by the atmospheric

421     BC load (anthropogenic only) in the entire atmospheric column but without North American (NAM)

422     contribution. With NAM contribution included in the simulation, the atmospheric BC is overestimated before

423     1980 resulting in a flat or a slightly downward trend for the period 1910-1970, unlike to the ice core rBC trend.

424     However, the good agreement between long-term rBC changes of Greenland ice core and modeled BC

deposition in Greenland using a chemistry-climate model with an input of ACCMIP BC inventory confirm that BC emission estimates for NAM from the ACCMIP inventory correctly quantify anthropogenic BC emissions in North America (Lamarque et al., 2010). Consequently, the observed overestimation of NAM contribution for winter at the ELB site (Fig 9b) is likely due to an overestimation of NAM footprint density in the statistical process applied on FLEXPART simulation data. The stronger BC inputs from NAM might have contributed to the increased winter rBC concentrations of the ELB ice core at the beginning of 20$^{th}$ century, although it was not shown in our simulations. Finally, the estimated BC without NAM contribution is defined as the "best scenario" for winter time.

Despite the similar features between the ice core rBC record and the best scenario for the atmospheric load which support that anthropogenic BC increase in the 20$^{th}$ century is reflected in the ELB record, BC maximum time period is not in total agreement (Fig. 9a and b). Unlike the ice core rBC that already largely increased in 1960 and peaked in 1970 for both summer and winter, the atmospheric BC load remarkably increases only in 1980. Substantial BC increase of ELB and Western European (CDD and CG) ice cores since the mid-20th century reveals that BC emissions increased during that period at a wide regional European scale. In addition, the CDD record shows a large increase in sulfate concentration since the mid-20th century lasting until ~1980 (Preunkert et al., 2001; Preunkert and Legrand, 2013). Knowing that sulfate and BC are often co-emitted in anthropogenic emission sources, e.g., in industrial sectors, one can expect a large increase in European BC emissions in 1960-1980, as suggested by the ELB ice core rBC record. The reliability of historic emission inventories for BC is reported to be lower than for $SO_2$, CO and NOx emissions, particularly for the period prior to 2000 (Granier et al., 2011), which is due to the uncertainties on BC emission factors for coal, gasoline and diesel fuels in various sectors (differ by a factor of 10 or more in literatures) and activity data (Granier et al., 2011; Vignati et al., 2010). Thus, the lack of substantial increase in the atmospheric BC load for the period 1960s-1970s could be associated primarily with underestimated European anthropogenic BC emissions for this period (Fig. 8c and d).

Moreover, the ice core rBC record and the atmospheric BC load do not exhibit similar patterns after 1980. Decreasing rates of the ice core rBC are much slower after 1980 onward for both seasons than the atmospheric BC load (Fig. 9a and b). Furthermore, the summer rBC trend of the ELB ice core even increased since 2000, although such a trend cannot be reported conclusively for winter layers (Fig. 4). The recent economic growth in Eastern, and some part of Central, European countries (World Bank Group, 2016) can contribute to the enhancement in the release of BC and co-emitted pollutants. Some of Eastern European countries have kept increasing their sulfur emissions mainly from heat production and public electricity from 2000 onward (Vestreng et al., 2007). Thus, the increase in rBC deposition at the Elbrus site, mostly identified in summer, was probably related to enhanced emissions from anthropogenic sources located in Eastern and Central Europe. On the other side, many of Eastern European countries, such as Ukraine and European part Russia which are geographically close to the Mt. Elbrus, are the countries with the greatest land use for agriculture in Europe (Rabbinge and van Diepen, 2000), and thus emissions of smoke aerosols from their agricultural waste burning are expected to be significant in summer time (Barnaba et al., 2011; Bovchaliuk et al., 2013; Stohl et al., 2007). Large emissions of smoke aerosols over Eastern Europe from summer forest/agricultural fires have been recently reported (Barnaba et al., 2011; Bovchaliuk et al., 2013; Sciare et al., 2008; Yoon et al., 2011; Zhou et al., 2012) and burned area from Global Fire Emissions Database (GFED) (Giglio et al., 2010) increased over Eastern Europe for the period

12

465 2004-2008 (Yoon et al., 2014). These emissions of smoke aerosols in the Eastern part of Europe may have
466 contributed to the observed summer BC increase in the ELB ice cores. Thus, the recent trend of the ELB ice core
467 rBC turning upward probably indicates changes in both anthropogenic emissions and summer forest/peat fires
468 over Eastern part of Europe in 2000s, which is not well reflected in the inventories.

469 Given the large existing uncertainties in historic BC emission inventories available to date, our rBC record
470 reconstructed from a high-altitude Caucasus ice cores should be useful to better constrain BC emissions.
471 Specifically, our study highlights the need for improving BC emission inventories from the Eastern part of
472 Europe since 1960. Reliability of Western European BC emissions could be more specifically assessed by
473 investigating high-resolution BC records extracted from Western European ice cores that would be more
474 representative of Western European emissions.

475

476 **4 Conclusions**

477 A high-resolution rBC record reconstructed from ice cores drilled from a high-altitude Eastern European site in
478 Mt. Elbrus (ELB), Caucasus, reported for the first time the long-term evolutions of rBC mass concentrations and
479 size distributions in the European outflows over the past 189 years, i.e., between year 1825 and year 2013. The
480 rBC record at ELB was largely impacted by rBC emissions located in the Eastern part of Europe. A large
481 temporal variability in rBC mass concentration was observed at both seasonal and annual timescales. This record
482 was also unique to document long-term variability of BC in this region of Europe.

483 In the first-half of 20th century, rBC concentrations increased by a 1.5-fold than its level in the preindustrial era
484 (before 1850). The summer (winter) rBC concentrations increased by a 5-fold (3.3-fold) in 1960-1980, followed
485 by a decrease until ~2000 and a slight increase again since ~2000. Consistent increase in background levels,
486 since the beginning of 20th century, highlights that rBC background level in the atmosphere at ELB was also
487 significantly altered. We have also investigated the potential of size distributions of rBC particles in the ice cores
488 as a new proxy to bring additional information on rBC removal processes, seasonal transport patterns, and
489 emission sources.

490 We simulated the atmospheric load of BC aerosols which were transported from the European continent, mainly
491 Eastern part of Europe, by coupling transport simulations (FLEXPART) to 20th-century BC emission inventories
492 (ACCMIP and MACCity). Similar features were observed between the ELB ice core rBC mass concentration
493 record and the best scenario for the atmospheric BC load at the ELB site: a BC increase at the onset of the 20th
494 century and a subsequent decrease since ~1980. This estimation evidently supports that European anthropogenic
495 activities resulted in the BC increase over Europe since ~1900, which was also seen in elemental carbon (EC)
496 records of Western European ice cores (Legrand et al., 2007; Thevenon et al., 2009). However, some
497 disagreements were seen between the ELB ice core rBC and the best scenario for atmospheric BC load at ELB,
498 e.g., (i) the lack of strong increase in the best scenario for the period 1960s and 1970s, unlike the ice core record,
499 (ii) the different decreasing rates after 1980 and (iii) the slightly increasing trend of the rBC ELB ice core record
500 that was not shown in the estimation. An explanation for such discrepancy could be that rapid enhancement of
501 BC emissions over Europe since 1960 and the recent BC changes in the Eastern part of Europe may not be well
502 accounted for in the emission inventories.

503 Most atmospheric BC measurements have focused on western and northern Europe (e.g., McMeeking et al.,

504　2010; Reche et al., 2011; Reddington et al., 2013) despite of growing evidences of strong aerosol emissions in
505　the Eastern part of Europe (Asmi et al., 2011; Barnaba et al., 2011; Bovchaliuk et al., 2013). It is thus critically
506　important to deploy new studies (atmospheric monitoring and investigation of ice archives) with a more
507　comprehensive European view, including both Western and Eastern areas. We suggest that century-long ice cores
508　at multiple high-altitude European sites with a homogeneous or well cross-compared measurement techniques
509　are needed to better constrain past BC emissions, infer efficiency of present BC emission regulation, and help
510　establishing future regulations on BC emissions.

511

525

526　**References**

527　Asmi, A., Wiedensohler, A., Laj, P., Fjaeraa, A.-M., Sellegri, K., Birmili, W., Weingartner, E., Baltensperger, U.,
528　Zdimal, V., Zikova, N., Putaud, J.-P., Marinoni, A., Tunved, P., Hansson, H.-C., Fiebig, M., Kivekäs, N.,
529　Lihavainen, H., Asmi, E., Ulevicius, V., Aalto, P. P., Swietlicki, E., Kristensson, A., Mihalopoulos, N., Kalivitis,
530　N., Kalapov, I., Kiss, G., de Leeuw, G., Henzing, B., Harrison, R. M., Beddows, D., O'Dowd, C., Jennings, S. G.,
531　Flentje, H., Weinhold, K., Meinhardt, F., Ries, L. and Kulmala, M.: Number size distributions and seasonality of
532　submicron particles in Europe 2008–2009, Atmos. Chem. Phys., 11(11), 5505–5538, doi:10.5194/acp-11-5505-
533　2011, 2011.

534　Barbosa, P., San-Miguel-Ayanz, J., Camia, A., Gimeno, M., Lib- erta, G. and Schmuck, G.: Assessment of fire
535　damages in the EU Mediterranean Countries during the 2003 Forest Fire Campaign, Official Publication of the
536　European Commission, Ispra., 2004.

537　Barnaba, F., Angelini, F., Curci, G. and Gobbi, G. P.: An important fingerprint of wildfires on the European
538　aerosol load, Atmos. Chem. Phys., 11(20), 10487–10501, doi:10.5194/acp-11-10487-2011, 2011.

539　Bisiaux, M. M., Edwards, R., McConnell, J. R., Curran, M. A. J., Van Ommen, T. D., Smith, A. M., Neumann, T.
540　A., Pasteris, D. R., Penner, J. E. and Taylor, K.: Changes in black carbon deposition to Antarctica from two
541　high-resolution ice core records, 1850-2000 AD, Atmos. Chem. Phys., 12(9), 4107–4115, doi:10.5194/acp-12-
542　4107-2012, 2012a.

543　Bisiaux, M. M., Edwards, R., McConnell, J. R., Albert, M. R., Anschutz, H., Neumann, T. A., Isaksson, E. and

Penner, J. E.: Variability of black carbon deposition to the East Antarctic Plateau, 1800-2000 AD, Atmos. Chem. Phys., 12(8), 3799–3808, doi:10.5194/acp-12-3799-2012, 2012b.

Bond, T. C., Doherty, S. J., Fahey, D. W., Forster, P. M., Berntsen, T., DeAngelo, B. J., Flanner, M. G., Ghan, S., Kärcher, B., Koch, D., Kinne, S., Kondo, Y., Quinn, P. K., Sarofim, M. C., Schultz, M. G., Schulz, M., Venkataraman, C., Zhang, H., Zhang, S., Bellouin, N., Guttikunda, S. K., Hopke, P. K., Jacobson, M. Z., Kaiser, J. W., Klimont, Z., Lohmann, U., Schwarz, J. P., Shindell, D., Storelvmo, T., Warren, S. G. and Zender, C. S.: Bounding the role of black carbon in the climate system: A scientific assessment, J. Geophys. Res. Atmos., 118(11), 5380–5552, doi:10.1002/jgrd.50171, 2013.

Bovchaliuk, A., Milinevsky, G., Danylevsky, V., Goloub, P., Dubovik, O., Holdak, A., Ducos, F. and Sosonkin, M.: Variability of aerosol properties over Eastern Europe observed from ground and satellites in the period from 2003 to 2011, Atmos. Chem. Phys., 13(13), 6587–6602, doi:10.5194/acp-13-6587-2013, 2013.

Bukowiecki, N., Weingartner, E., Gysel, M., Collaud Coen, M., Zieger, P., Herrmann, E., Steinbacher, M., Gäggeler, H. W. and and Baltensperger, U.: A Review of More Than 20 Years of Aerosol Observation at the High Altitude Research Station Jungfraujoch, Switzerland (3580masl), Aerosol Air Qual. Res., 16(3), 764–788, doi:10.4209/aaqr.2015.05.0305, 2016.

Dahlkötter, F., Gysel, M., Sauer, D., Minikin, A., Baumann, R., Seifert, P., Ansmann, A., Fromm, M., Voigt, C. and Weinzierl, B.: The Pagami Creek smoke plume after long-range transport to the upper troposphere over Europe – aerosol properties and black carbon mixing state, Atmos. Chem. Phys., 14(12), 6111–6137, doi:10.5194/acp-14-6111-2014, 2014.

Diehl, T., Heil, A., Chin, M., Pan, X., Streets, D., Schultz, M. and Kinne, S.: Anthropogenic, biomass burning, and volcanic emissions of black carbon, organic carbon, and SO2 from 1980 to 2010 for hindcast model experiments, Atmos. Chem. Phys. Discuss., 12(9), 24895–24954, doi:10.5194/acpd-12-24895-2012, 2012.

Fagerli, H., Legrand, M., Preunkert, S., Vestreng, V., Simpson, D. and Cerqueira, M.: Modeling historical long-term trends of sulfate, ammonium, and elemental carbon over Europe: A comparison with ice core records in the Alps, J. Geophys. Res., 112(D23), D23S13, doi:10.1029/2006JD008044, 2007.

Flanner, M. G., Zender, C. S., Randerson, J. T. and Rasch, P. J.: Present-day climate forcing and response from black carbon in snow, J. Geophys. Res., 112(D11), doi:Artn D11202 Doi 10.1029/2006jd008003, 2007.

Forster, C., Stohl, A. and Seibert, P.: Parameterization of Convective Transport in a Lagrangian Particle Dispersion Model and Its Evaluation, J. Appl. Meteorol. Climatol., 46(4), 403–422, doi:10.1175/JAM2470.1, 2007.

Giglio, L., Randerson, J. T., van der Werf, G. R., Kasibhatla, P. S., Collatz, G. J., Morton, D. C. and DeFries, R. S.: Assessing variability and long-term trends in burned area by merging multiple satellite fire products, Biogeosciences, 7(3), 1171–1186, doi:10.5194/bg-7-1171-2010, 2010.

Ginot, P., Dumont, M., Lim, S., Patris, N., Taupin, J.-D., Wagnon, P., Gilbert, A., Arnaud, Y., Marinoni, A., Bonasoni, P. and Laj, P.: A 10 year record of black carbon and dust from a Mera Peak ice core (Nepal): variability and potential impact on melting of Himalayan glaciers, Cryosph., 8(4), 1479–1496, doi:10.5194/tc-8-1479-2014, 2014.

Granier, C., Bessagnet, B., Bond, T. C., D'Angiola, A., Denier van der Gon, H., Frost, G. J., Heil, A., Kaiser, J. W., Kinne, S., Klimont, Z., Kloster, S., Lamarque, J.-F., Liousse, C., Masui, T., Meleux, F., Mieville, A., Ohara, T., Raut, J.-C., Riahi, K., Schultz, M. G., Smith, S. J., Thompson, A., Aardenne, J., Werf, G. R. and Vuuren, D.

584    P.: Evolution of anthropogenic and biomass burning emissions of air pollutants at global and regional scales

585    during the 1980–2010 period, Clim. Change, 109(1–2), 163–190, doi:10.1007/s10584-011-0154-1, 2011.

586    Guilhermet, J., Preunkert, S., Voisin, D., Baduel, C. and Legrand, M.: Major 20th century changes of water-

587    soluble humic-like substances (HULIS WS ) aerosol over Europe inferred from Alpine ice cores, J. Geophys.

588    Res. Atmos., 118(9), 3869–3878, doi:10.1002/jgrd.50201, 2013.

589    Hansen, J. and Nazarenko, L.: Soot climate forcing via snow and ice albedos, Proc. Natl. Acad. Sci. U. S. A.,

590    101(2), 423–428, doi:DOI 10.1073/pnas.2237157100, 2004.

591    Hodzic, A., Vautard, R., Chepfer, H., Goloub, P., Menut, L., Chazette, P., Deuzé, J. L., Apituley, A. and Couvert,

592    P.: Evolution of aerosol optical thickness over Europe during the August 2003 heat wave as seen from

593    CHIMERE model simulations and POLDER data, Atmos. Chem. Phys., 6(7), 1853–1864, doi:10.5194/acp-6-

594    1853-2006, 2006.

595    Jenk, T. M., Szidat, S., Schwikowski, M., Gaggeler, H. W., Brutsch, S., Wacker, L., Synal, H. A. and Saurer, M.:

596    Radiocarbon analysis in an Alpine ice core: record of anthropogenic and biogenic contributions to carbonaceous

597    aerosols in the past (1650-1940), Atmos. Chem. Phys., 6, 5381–5390, doi:10.5194/acp-6-5381-2006, 2006.

598    Jenkins, M., Kaspari, S., Kang, S., Grigholm, B. and Mayewski, P. A.: Black carbon concentrations from a

599    Tibetan Plateau ice core spanning 1843–1982: recent increases due to emissions and glacier melt, Cryosph.

600    Discuss., 7(5), 4855–4880, doi:10.5194/tcd-7-4855-2013, 2013.

601    Kaspari, S., Painter, T. H., Gysel, M., Skiles, S. M. and Schwikowski, M.: Seasonal and elevational variations of

602    black carbon and dust in snow and ice in the Solu-Khumbu, Nepal and estimated radiative forcings, Atmos.

603    Chem. Phys., 14(15), 8089–8103, doi:10.5194/acp-14-8089-2014, 2014.

604    Kaspari, S. D., Schwikowski, M., Gysel, M., Flanner, M. G., Kang, S., Hou, S. and Mayewski, P. A.: Recent

605    increase in black carbon concentrations from a Mt. Everest ice core spanning 1860-2000 AD, Geophys. Res.

606    Lett., 38, doi:Artn L04703 Doi 10.1029/2010gl046096, 2011.

607    Kondo, Y., Sahu, L., Moteki, N., Khan, F., Takegawa, N., Liu, X., Koike, M. and Miyakawa, T.: Consistency

608    and Traceability of Black Carbon Measurements Made by Laser-Induced Incandescence, Thermal-Optical

609    Transmittance, and Filter-Based Photo-Absorption Techniques, Aerosol Sci. Technol., 45(2), 295–312,

610    doi:10.1080/02786826.2010.533215, 2011a.

611    Kondo, Y., Matsui, H., Moteki, N., Sahu, L., Takegawa, N., Kajino, M., Zhao, Y., Cubison, M. J., Jimenez, J. L.,

612    Vay, S., Diskin, G. S., Anderson, B., Wisthaler, A., Mikoviny, T., Fuelberg, H. E., Blake, D. R., Huey, G.,

613    Weinheimer, A. J., Knapp, D. J. and Brune, W. H.: Emissions of black carbon, organic, and inorganic aerosols

614    from biomass burning in North America and Asia in 2008, J. Geophys. Res., 116(D8), D08204,

615    doi:10.1029/2010JD015152, 2011b.

616    Kozachek, A., Mikhalenko, V., Masson-Delmotte, V., Ekaykin, A., Ginot, P., Kutuzov, S., Legrand, M.,

617    Lipenkov, V. and Preunkert, S.: Large-scale drivers of Caucasus climate variability in meteorological records

618    and Mt Elbrus ice cores, Clim. Past Discuss., 1–30, doi:10.5194/cp-2016-62, 2016.

619    Laborde, M., Schnaiter, M., Linke, C., Saathoff, H., Naumann, K.-H., Möhler, O., Berlenz, S., Wagner, U.,

620    Taylor, J. W., Liu, D., Flynn, M., Allan, J. D., Coe, H., Heimerl, K., Dahlkötter, F., Weinzierl, B., Wollny, A. G.,

621    Zanatta, M., Cozic, J., Laj, P., Hitzenberger, R., Schwarz, J. P. and Gysel, M.: Single Particle Soot Photometer

622    intercomparison at the AIDA chamber, Atmos. Meas. Tech., 5, 3077–3097, doi:10.5194/amt-5-3077-2012, 2012.

623    Laborde, M., Crippa, M., Tritscher, T., Jurányi, Z., Decarlo, P. F., Temime-Roussel, B., Marchand, N., Eckhardt,

624    S., Stohl, A., Baltensperger, U., Prévôt, A. S. H., Weingartner, E. and Gysel, M.: Black carbon physical

625    properties and mixing state in the European megacity Paris, Atmos. Chem. Phys., 13(11), 5831–5856,

626    doi:10.5194/acp-13-5831-2013, 2013.

627    Lamarque, J.-F., Bond, T. C., Eyring, V., Granier, C., Heil, A., Klimont, Z., Lee, D., Liousse, C., Mieville, A.,

628    Owen, B., Schultz, M. G., Shindell, D., Smith, S. J., Stehfest, E., Van Aardenne, J., Cooper, O. R., Kainuma, M.,

629    Mahowald, N., McConnell, J. R., Naik, V., Riahi, K. and van Vuuren, D. P.: Historical (1850–2000) gridded

630    anthropogenic and biomass burning emissions of reactive gases and aerosols: methodology and application,

631    Atmos. Chem. Phys., 10(15), 7017–7039, doi:10.5194/acp-10-7017-2010, 2010.

632    Lavanchy, V. M. H., Gäggeler, H. W., Schotterer, U., Schwikowski, M. and Baltensperger, U.: Historical record

633    of carbonaceous particle concentrations from a European high-alpine glacier (Colle Gnifetti, Switzerland), J.

634    Geophys. Res. Atmos., 104(D17), 21227–21236, doi:10.1029/1999jd900408, 1999.

635    Legrand, M., Preunkert, S., Schock, M., Cerqueira, M., Kasper-Giebl, A., Afonso, J., Pio, C., Gelencsér, A. and

636    Dombrowski-Etchevers, I.: Major 20th century changes of carbonaceous aerosol components (EC, WinOC,

637    DOC, HULIS, carboxylic acids, and cellulose) derived from Alpine ice cores, J. Geophys. Res., 112(D23),

638    D23S11, doi:10.1029/2006jd008080, 2007.

639    Legrand, M., Preunkert, S., May, B., Guilhermet, J., Hoffman, H. and Wagenbach, D.: Major 20th century

640    changes of the content and chemical speciation of organic carbon archived in Alpine ice cores: Implications for

641    the long-term change of organic aerosol over Europe, J. Geophys. Res. Atmos., 118(9), 3879–3890,

642    doi:10.1002/jgrd.50202, 2013.

643    Lim, S., Faïn, X., Zanatta, M., Cozic, J., Jaffrezo, J.-L., Ginot, P. and Laj, P.: Refractory black carbon mass

644    concentrations in snow and ice: method evaluation and inter-comparison with elemental carbon measurement,

645    Atmos. Meas. Tech., 7(10), 3307–3324, doi:10.5194/amt-7-3307-2014, 2014.

646    Liu, D., Flynn, M., Gysel, M., Targino, A., Crawford, I., Bower, K., Choularton, T., Jurányi, Z., Steinbacher, M.,

647    Hüglin, C., Curtius, J., Kampus, M., Petzold, A., Weingartner, E., Baltensperger, U. and Coe, H.: Single particle

648    characterization of black carbon aerosols at a tropospheric alpine site in Switzerland, Atmos. Chem. Phys.,

649    10(15), 7389–7407, doi:10.5194/acp-10-7389-2010, 2010.

650    Lugauer, M., Baltensperger, U., Furger, M., Gäggeler, H. W., Jost, D. T., Schwikowski, M. and Wanner, H.:

651    Aerosol transport to the high Alpine sites Jungfraujoch (3454 m asl) and Colle Gnifetti (4452 m asl), Tellus B,

652    50(1), doi:10.3402/tellusb.v50i1.16026, 1998.

653    Luterbacher, J., Dietrich, D., Xoplaki, E., Grosjean, M. and Wanner, H.: European seasonal and annual

654    temperature variability, trends, and extremes since 1500., Science, 303(5663), 1499–503,

655    doi:10.1126/science.1093877, 2004.

656    Matthias, V. and Bösenberg, J.: Aerosol climatology for the planetary boundary layer derived from regular lidar

657    measurements, Atmos. Res., 63(3–4), 221–245, doi:10.1016/S0169-8095(02)00043-1, 2002.

658    Matthias, V., Balis, D., Bösenberg, J., Eixmann, R., Iarlori, M., Komguem, L., Mattis, I., Papayannis, A.,

659    Pappalardo, G., Perrone, M. R. and Wang, X.: Vertical aerosol distribution over Europe: Statistical analysis of

660    Raman lidar data from 10 European Aerosol Research Lidar Network (EARLINET) stations, J. Geophys. Res.,

661    109(D18), D18201, doi:10.1029/2004JD004638, 2004.

662    McConnell, J. R., Edwards, R., Kok, G. L., Flanner, M. G., Zender, C. S., Saltzman, E. S., Banta, J. R., Pasteris,

663    D. R., Carter, M. M. and Kahl, J. D. W.: 20th-century industrial black carbon emissions altered arctic climate

forcing, Science (80)., 317(5843), 1381–1384, doi:10.1126/science.1144856, 2007.

McMeeking, G. R., Hamburger, T., Liu, D., Flynn, M., Morgan, W. T., Northway, M., Highwood, E. J., Krejci, R., Allan, J. D., Minikin, A. and Coe, H.: Black carbon measurements in the boundary layer over western and northern Europe, Atmos. Chem. Phys., 10(19), 9393–9414, doi:10.5194/acp-10-9393-2010, 2010.

Mikhalenko, V., Sokratov, S., Kutuzov, S., Ginot, P., Legrand, M., Preunkert, S., Lavrentiev, I., Kozachek, A., Ekaykin, A., Faïn, X., Lim, S., Schotterer, U., Lipenkov, V. and Toropov, P.: Investigation of a deep ice core from the Elbrus western plateau, the Caucasus, Russia, Cryosph., 9(6), 2253–2270, doi:10.5194/tc-9-2253-2015, 2015.

Miyakawa, T., Kanaya, Y., Komazaki, Y., Taketani, F., Pan, X., Irwin, M. and Symonds, J.: Intercomparison between a single particle soot photometer and evolved gas analysis in an industrial area in Japan: Implications for the consistency of soot aerosol mass concentration measurements, Atmos. Environ., 127, 14–21, doi:10.1016/j.atmosenv.2015.12.018, 2016.

Mori, T., Moteki, N., Ohata, S., Koike, M., Goto-Azuma, K., Miyazaki, Y. and Kondo, Y.: Improved technique for measuring the size distribution of black carbon particles in liquid water, Aerosol Sci. Technol., 50(3), 242–254, doi:10.1080/02786826.2016.1147644, 2016.

Moteki, N. and Kondo, Y.: Dependence of Laser-Induced Incandescence on Physical Properties of Black Carbon Aerosols: Measurements and Theoretical Interpretation, Aerosol Sci. Technol., 44(8), 663–675, doi:10.1080/02786826.2010.484450, 2010.

Moteki, N., Kondo, Y., Oshima, N., Takegawa, N., Koike, M., Kita, K., Matsui, H. and Kajino, M.: Size dependence of wet removal of black carbon aerosols during transport from the boundary layer to the free troposphere, Geophys. Res. Lett., 39(13), doi:10.1029/2012GL052034, 2012.

Petzold, A., Ogren, J. A., Fiebig, M., Laj, P., Li, S.-M., Baltensperger, U., Holzer-Popp, T., Kinne, S., Pappalardo, G., Sugimoto, N., Wehrli, C., Wiedensohler, A. and Zhang, X.-Y.: Recommendations for reporting "black carbon" measurements, Atmos. Chem. Phys., 13(16), 8365–8379, doi:10.5194/acp-13-8365-2013, 2013.

Pio, C. A., Legrand, M., Oliveira, T., Afonso, J., Santos, C., Caseiro, A., Fialho, P., Barata, F., Puxbaum, H., Sanchez-Ochoa, A., Kasper-Giebl, A., Gelencsér, A., Preunkert, S. and Schock, M.: Climatology of aerosol composition (organic versus inorganic) at nonurban sites on a west-east transect across Europe, J. Geophys. Res., 112(D23), D23S02, doi:10.1029/2006JD008038, 2007.

Preunkert, S. and Legrand, M.: Towards a quasi-complete reconstruction of past atmospheric aerosol load and composition (organic and inorganic) over Europe since 1920 inferred from Alpine ice cores, Clim. Past, 9(4), 1403–1416, doi:10.5194/cp-9-1403-2013, 2013.

Preunkert, S., Wagenbach, D., Legrand, M. and Vincent, C.: Col du Dôme (Mt Blanc Massif, French Alps) suitability for ice-core studies in relation with past atmospheric chemistry over Europe, Tellus B, 52(3), 993–1012, doi:10.1034/j.1600-0889.2000.d01-8.x, 2000.

Preunkert, S., Legrand, M. and Wagenbach, D.: Sulfate trends in a Col du Dôme (French Alps) ice core: A record of anthropogenic sulfate levels in the European midtroposphere over the twentieth century, J. Geophys. Res. Atmos., 106(D23), 31991–32004, doi:10.1029/2001JD000792, 2001.

Rabbinge, R. and van Diepen, C. A.: Changes in agriculture and land use in Europe, Eur. J. Agron., 13(2–3), 85–99, doi:10.1016/S1161-0301(00)00067-8, 2000.

Ramanathan, V. and Carmichael, G.: Global and regional climate changes due to black carbon, Nat. Geosci, 1(4),

221–227, 2008.

Reche, C., Querol, X., Alastuey, A., Viana, M., Pey, J., Moreno, T., Rodríguez, S., González, Y., Fernández-Camacho, R., de la Rosa, J., Dall'Osto, M., Prévôt, A. S. H., Hueglin, C., Harrison, R. M. and Quincey, P.: New considerations for PM, Black Carbon and particle number concentration for air quality monitoring across different European cities, Atmos. Chem. Phys., 11(13), 6207–6227, doi:10.5194/acp-11-6207-2011, 2011.

Reddington, C. L., McMeeking, G., Mann, G. W., Coe, H., Frontoso, M. G., Liu, D., Flynn, M., Spracklen, D. V. and Carslaw, K. S.: The mass and number size distributions of black carbon aerosol over Europe, Atmos. Chem. Phys., 13(9), 4917–4939, doi:10.5194/acp-13-4917-2013, 2013.

Schär, C., Vidale, P. L., Lüthi, D., Frei, C., Häberli, C., Liniger, M. A. and Appenzeller, C.: The role of increasing temperature variability in European summer heatwaves., Nature, 427(6972), 332–6, doi:10.1038/nature02300, 2004.

Schwarz, J. P., Gao, R. S., Fahey, D. W., Thomson, D. S., Watts, L. a., Wilson, J. C., Reeves, J. M., Darbeheshti, M., Baumgardner, D. G., Kok, G. L., Chung, S. H., Schulz, M., Hendricks, J., Lauer, a., Kärcher, B., Slowik, J. G., Rosenlof, K. H., Thompson, T. L., Langford, a. O., Loewenstein, M. and Aikin, K. C.: Single-particle measurements of midlatitude black carbon and light-scattering aerosols from the boundary layer to the lower stratosphere, J. Geophys. Res., 111(D16), D16207, doi:10.1029/2006JD007076, 2006.

Schwarz, J. P., Gao, R. S., Spackman, J. R., Watts, L. A., Thomson, D. S., Fahey, D. W., Ryerson, T. B., Peischl, J., Holloway, J. S., Trainer, M., Frost, G. J., Baynard, T., Lack, D. A., de Gouw, J. A., Warneke, C. and Del Negro, L. A.: Measurement of the mixing state, mass, and optical size of individual black carbon particles in urban and biomass burning emissions, Geophys. Res. Lett., 35(13), L13810, doi:10.1029/2008GL033968, 2008.

Schwarz, J. P., Doherty, S. J., Li, F., Ruggiero, S. T., Tanner, C. E., Perring, A. E., Gao, R. S. and Fahey, D. W.: Assessing Single Particle Soot Photometer and Integrating Sphere/Integrating Sandwich Spectrophotometer measurement techniques for quantifying black carbon concentration in snow, Atmos. Meas. Tech., 5(11), 2581–2592, doi:10.5194/amt-5-2581-2012, 2012.

Schwarz, J. P., Gao, R. S., Perring, A. E., Spackman, J. R. and Fahey, D. W.: Black carbon aerosol size in snow., Sci. Rep., 3, 1356, doi:10.1038/srep01356, 2013.

Sciare, J., Oikonomou, K., Favez, O., Markaki, Z., Liakakou, E., Cachier, H. and Mihalopoulos, N.: Long-term measurements of carbonaceous aerosols in the eastern Mediterranean: evidence of long-range transport of biomass burning, Atmos. Chem. Phys. Discuss., 8(2), 6949–6982, doi:10.5194/acpd-8-6949-2008, 2008.

Seibert, P. and Frank, a.: Source-receptor matrix calculation with a Lagrangian particle dispersion model in backward mode, Atmos. Chem. Phys., 4(1), 51–63, doi:10.5194/acp-4-51-2004, 2004.

Stephens, M., Turner, N. and Sandberg, J.: Particle identification by laser-induced incandescence in a solid-state laser cavity., Appl. Opt., 42(19), 3726–3736, 2003.

Stohl, A. and Thomson, D. J.: A Density Correction for Lagrangian Particle Dispersion Models, Boundary-Layer Meteorol., 90(1), 155–167, doi:10.1023/A:1001741110696, 1999.

Stohl, A., Forster, C., Frank, A., Seibert, P. and Wotawa, G.: Technical note: The Lagrangian particle dispersion model FLEXPART version 6.2, Atmos. Chem. Phys., 5(9), 2461–2474, doi:10.5194/acp-5-2461-2005, 2005.

Stohl, A., Berg, T., Burkhart, J. F., Fjǽraa, A. M., Forster, C., Herber, A., Hov, Ø., Lunder, C., McMillan, W. W., Oltmans, S., Shiobara, M., Simpson, D., Solberg, S., Stebel, K., Ström, J., Tørseth, K., Treffeisen, R., Virkkunen, K. and Yttri, K. E.: Arctic smoke – record high air pollution levels in the European Arctic due to agricultural

744    fires in Eastern Europe in spring 2006, Atmos. Chem. Phys., 7(2), 511–534, doi:10.5194/acp-7-511-2007, 2007.

745    Taylor, J. W., Allan, J. D., Allen, G., Coe, H., Williams, P. I., Flynn, M. J., Le Breton, M., Muller, J. B. A.,

746    Percival, C. J., Oram, D., Forster, G., Lee, J. D., Rickard, A. R., Parrington, M. and Palmer, P. I.: Size-dependent

747    wet removal of black carbon in Canadian biomass burning plumes, Atmos. Chem. Phys., 14(24), 13755–13771,

748    doi:10.5194/acp-14-13755-2014, 2014.

749    Thevenon, F., Anselmetti, F. S., Bernasconi, S. M. and Schwikowski, M.: Mineral dust and elemental black

750    carbon records from an Alpine ice core (Colle Gnifetti glacier) over the last millennium, J. Geophys. Res., 114,

751    doi:D17102 10.1029/2008jd011490, 2009.

752    Tørseth, K., Aas, W., Breivik, K., Fjæraa, A. M., Fiebig, M., Hjellbrekke, A. G., Lund Myhre, C., Solberg, S.

753    and Yttri, K. E.: Introduction to the European Monitoring and Evaluation Programme (EMEP) and observed

754    atmospheric composition change during 1972–2009, Atmos. Chem. Phys., 12(12), 5447–5481, doi:10.5194/acp-

755    12-5447-2012, 2012.

756    Tsyro, S., Simpson, D., Tarrasón, L., Klimont, Z., Kupiainen, K., Pio, C. and Yttri, K. E.: Modeling of elemental

757    carbon over Europe, J. Geophys. Res., 112(D23), D23S19, doi:10.1029/2006JD008164, 2007.

758    Venzac, H., Sellegri, K., Villani, P., Picard, D. and Laj, P.: Seasonal variation of aerosol size distributions in the

759    free troposphere and residual layer at the puy de Dôme station, France, Atmos. Chem. Phys., 9(4), 1465–1478,

760    doi:10.5194/acp-9-1465-2009, 2009.

761    Vestreng, V., Myhre, G., Fagerli, H., Reis, S. and Tarrasón, L.: Twenty-five years of continuous sulphur dioxide

762    emission reduction in Europe, Atmos. Chem. Phys., 7(13), 3663–3681, doi:10.5194/acp-7-3663-2007, 2007.

763    Vignati, E., Karl, M., Krol, M., Wilson, J., Stier, P. and Cavalli, F.: Sources of uncertainties in modelling black

764    carbon at the global scale, Atmos. Chem. Phys., 10(6), 2595–2611, doi:10.5194/acp-10-2595-2010, 2010.

765    Wang, M., Xu, B., Kaspari, S. D., Gleixner, G., Schwab, V. F., Zhao, H., Wang, H. and Yao, P.: Century-long

766    record of black carbon in an ice core from the Eastern Pamirs: Estimated contributions from biomass burning,

767    Atmos. Environ., 115, 79–88, doi:10.1016/j.atmosenv.2015.05.034, 2015.

768    Wendl, I. A., Menking, J. A., Färber, R., Gysel, M., Kaspari, S. D., Laborde, M. J. G. and Schwikowski, M.:

769    Optimized method for black carbon analysis in ice and snow using the Single Particle Soot Photometer, Atmos.

770    Meas. Tech. Discuss., 7(3), 3075–3111, doi:10.5194/amtd-7-3075-2014, 2014.

771    van der Werf, G. R., Randerson, J. T., Giglio, L., Collatz, G. J., Kasibhatla, P. S. and Arellano, A. F.: Interannual

772    variability in global biomass burning emissions from 1997 to 2004, Atmos. Chem. Phys., 6(11), 3423–3441,

773    doi:10.5194/acp-6-3423-2006, 2006.

774    van der Werf, G. R., Randerson, J. T., Giglio, L., Collatz, G. J., Mu, M., Kasibhatla, P. S., Morton, D. C.,

775    DeFries, R. S., Jin, Y. and van Leeuwen, T. T.: Global fire emissions and the contribution of deforestation,

776    savanna, forest, agricultural, and peat fires (1997–2009), Atmos. Chem. Phys., 10(23), 11707–11735,

777    doi:10.5194/acp-10-11707-2010, 2010.

778    World Bank Group, M.: The World Bank Data, 2016.

779    Xu, Y., Ramanathan, V. and Washington, W. M.: Observed high-altitude warming and snow cover retreat over

780    Tibet and the Himalayas enhanced by black carbon aerosols, Atmos. Chem. Phys., 16(3), 1303–1315,

781    doi:10.5194/acp-16-1303-2016, 2016.

782    Yoon, J., von Hoyningen-Huene, W., Vountas, M. and Burrows, J. P.: Analysis of linear long-term trend of

783    aerosol optical thickness derived from SeaWiFS using BAER over Europe and South China, Atmos. Chem.

784    Phys., 11(23), 12149–12167, doi:10.5194/acp-11-12149-2011, 2011.

785    Yoon, J., Burrows, J. P., Vountas, M., von Hoyningen-Huene, W., Chang, D. Y., Richter, A. and Hilboll, A.:

786    Changes in atmospheric aerosol loading retrieved from space-based measurements during the past decade,

787    Atmos. Chem. Phys., 14(13), 6881–6902, doi:10.5194/acp-14-6881-2014, 2014.

788    Yttri, K. E., Aas, W., Bjerke, A., Cape, J. N., Cavalli, F., Ceburnis, D., Dye, C., Emblico, L., Facchini, M. C.,

789    Forster, C., Hanssen, J. E., Hansson, H. C., Jennings, S. G., Maenhaut, W., Putaud, J. P. and Tørseth, K.:

790    Elemental and organic carbon in PM10: a one year measurement campaign within the European Monitoring and

791    Evaluation Programme EMEP, Atmos. Chem. Phys., 7(22), 5711–5725, doi:10.5194/acp-7-5711-2007, 2007.

792    Zhou, C., Penner, J. E., Flanner, M. G., Bisiaux, M. M., Edwards, R. and McConnell, J. R.: Transport of black

793    carbon to polar regions: Sensitivity and forcing by black carbon, Geophys. Res. Lett., 39(22), L22804,

794    doi:10.1029/2012gl053388, 2012.

795

796

797

798

799

800

801

802

803

804

805

806

807

808

809

810

811

812

813

814

815

816

817

818

819

820

821

822

823 **Table and figures**

824

825 **Tables**

826 **Table 1. rBC mass concentrations at seasonal resolution and relative increases compared to 1825-1850**

827 **(preindustrial era) for different time periods.**

| Time period | Summer | | Winter | |
|---|---|---|---|---|
| | Concentration in µg L$^{-1}$ (median ± SD) | Relative increase to 1825-1850 | Concentration in µg L$^{-1}$ (median ± SD) | Relative increase to 1825-1850 |
| 1825-1850 | 4.3±1.5 | 1.0 | 2.0±0.9 | 1.0 |
| 1850-1900 | 5.3±2.6 | 1.1 | 2.5±1.4 | 1.0 |
| 1900-1950 | 7.9±3.9 | 1.5 | 3.2±1.6 | 1.4 |
| 1950-2000 | 20.0±7.1 | 4.3 | 6.0±2.7 | 2.7 |
| 1960-1980 | 22.6±7.2 | 5.0 | 7.1±2.5 | 3.3 |
| 2000-2013 | 17.7±5.9 | 3.9 | 5.4±2.3 | 2.4 |

828
829
830
831
832
833
834
835
836
837
838
839
840
841
842
843
844
845
846
847
848
849
850
851
852

**Figure 1.** Location of the ice core drilling site (43°20'53, 9"N, 42°25'36, 0"E, 5115 m a.s.l., indicated by the red star or arrow) in the Mt. Elbrus, the western Caucasus mountain range between the Black and the Caspian seas.

**Figure 2.** Five sub-regions classified as potential rBC emission source regions. Elbrus drilling site is indicated by a red circle. WEU, CEU, EEU, NAF and NAM represent Western Europe, Central Europe, Eastern Europe, North Africa and North America, respectably.

**Figure 3.** A Profile of high-resolution rBC concentration of Mt. Elbrus ice cores. (a) Whole rBC profile of both the 2013 core and the 2009 core, and (b) the 2009 core from top to 20 m corresponding to the blue region in (a). In (b), lower resolution (at ~5-10 cm resolution; black color) and high resolution (at 1 cm resolution; red color) rBC profiles obtained from discrete analysis and continuous flow analysis, respectively, are shown. For a whole rBC record, a section of lower-resolution signals of the 2009 core (corresponding to calendar year 2009) was replaced with the high-resolution rBC signals of the 2013 core. Gray text on top of figures stands for calendar year corresponding to ice core depth.

**Figure 4.** Annually averaged temporal evolution in rBC mass concentration of the ELB ice cores. (a) Summer, (b) winter, and (c) annual variabilities. Thin solid line is medians and dashed lines are lower and upper $10^{th}$ percentiles of the seasonal or annual rBC values. Upper $10^{th}$ percentiles do not exceed 75 μg L$^{-1}$, 35 μg L$^{-1}$, and 56 μg L$^{-1}$ for summer, winter, and annual, respectively. Thick lines are 10-year smoothing of medians. Discontinuous thin lines indicate ice layers with unclear seasonality or unanalyzed ice layers. Note different y-scales for three time series of rBC concentrations.

**Figure 5.** Time series of mass mode diameter (MMD) of seasonal rBC size distributions for the period of 1940-2009. The MMD was obtained by fitting a log-normal curve to the measured distribution. Horizontal lines stand for geometric means for summer (red) and winter (blue).

**Figure 6.** Air mass footprint area for (a) June to August (JJA) and (b) December to February (DJF) in the atmospheric column and (c) JJA in the lowest 2 km in the atmosphere. Color bar on the left indicates footprints density with a process defined unit (p.d.u.). The location of the ELB site is marked by a white triangle. JJA and DJF correspond to summer and winter of the ELB ice core depth, respectively.

**Figure 7.** Contribution of each regional footprint density (%) for (a) JJA and (b) DJF in the atmospheric column and (c) JJA in the lowest 2 km in the atmosphere. Footprint density of each region is divided by the footprint density of the entire footprint area (EEU+CEU+WEU+NAF+NAM+Others) and then described in percentage. Information for each region is found in the Sect. 2.4.

**Figure 8.** Historic regional BC emissions and atmospheric BC load at ELB for the period 1900-2008. In (a) and (b), anthropogenic and biomass burning (forest fires and savanna burning) BC emissions estimated by ACCMIP and MACCity (Diehl et al., 2012; Granier et al., 2011; Lamarque et al., 2010; van der Werf et al., 2006). In (c) and (d), atmospheric BC load (Tg yr$^{-1}$) is calculated by multiplying decadal-scale BC emissions in each region (a and b) by its relative contribution to the entire footprint area of ELB site (figure 7). In (c), both anthropogenic and biomass burning emissions are used for the reconstruction in JJA, as this type of biomass burning (forest fires and savanna burning) is the most frequent in summer and in (d), only anthropogenic emissions are used for DJF. Details are found in the text.

**Figure 9.** Comparison in temporal evolution between the rBC mass concentration of the ELB ice core and the estimates of atmospheric BC load at the ELB site, on a decadal scale. (a) JJA and (b) DJF. Best scenarios for

893 atmospheric BC load are shown in black thick lines. In (b), NAM stands for North America. See the text and
894 Figure 8c and d for calculations of the atmospheric BC load.

895

896 **Figures**
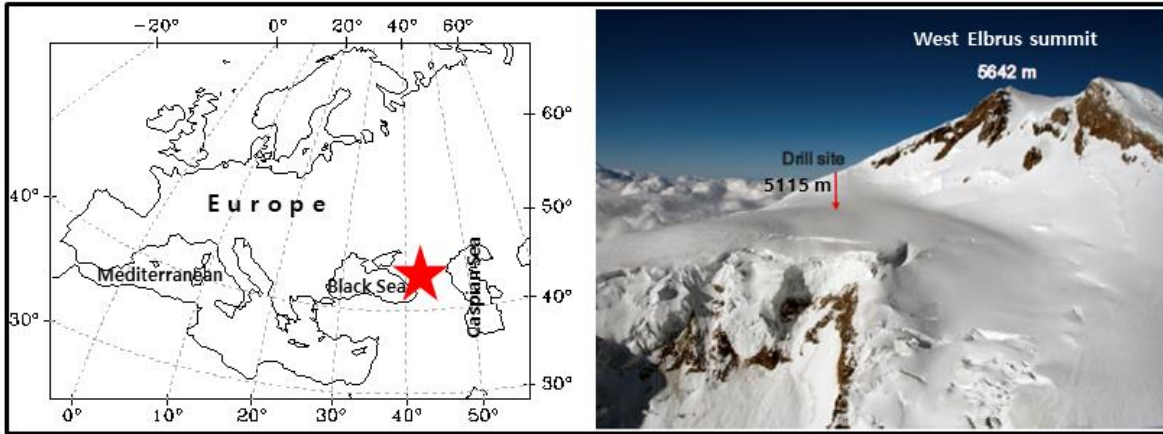


897

898 **Figure 1**

899

900

901

902

903
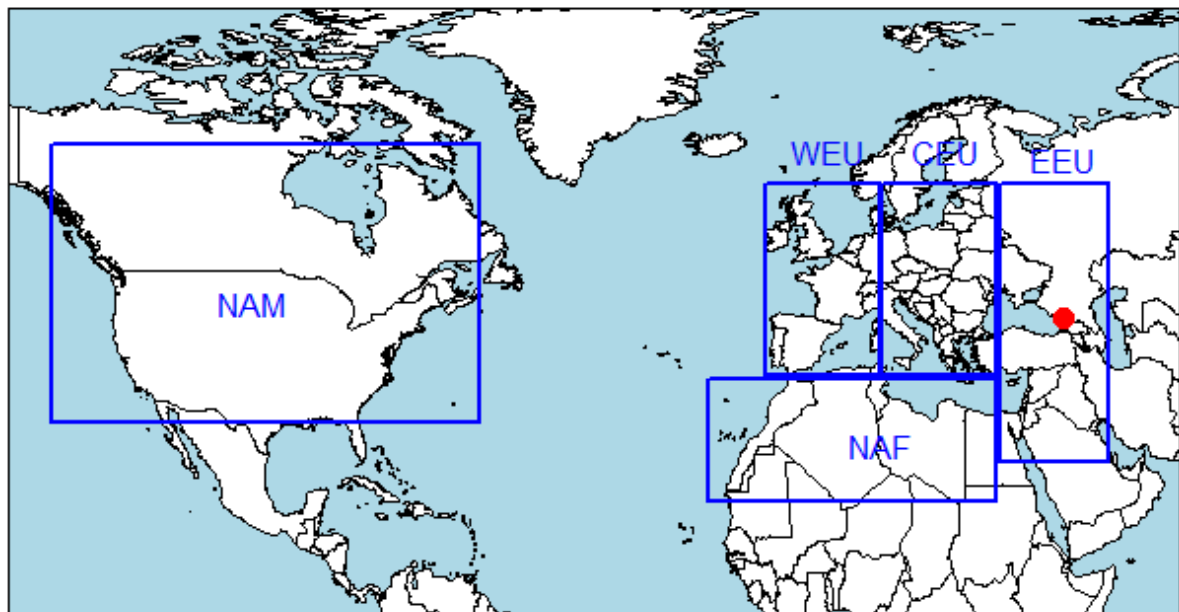


904

905 **Figure 2**

906
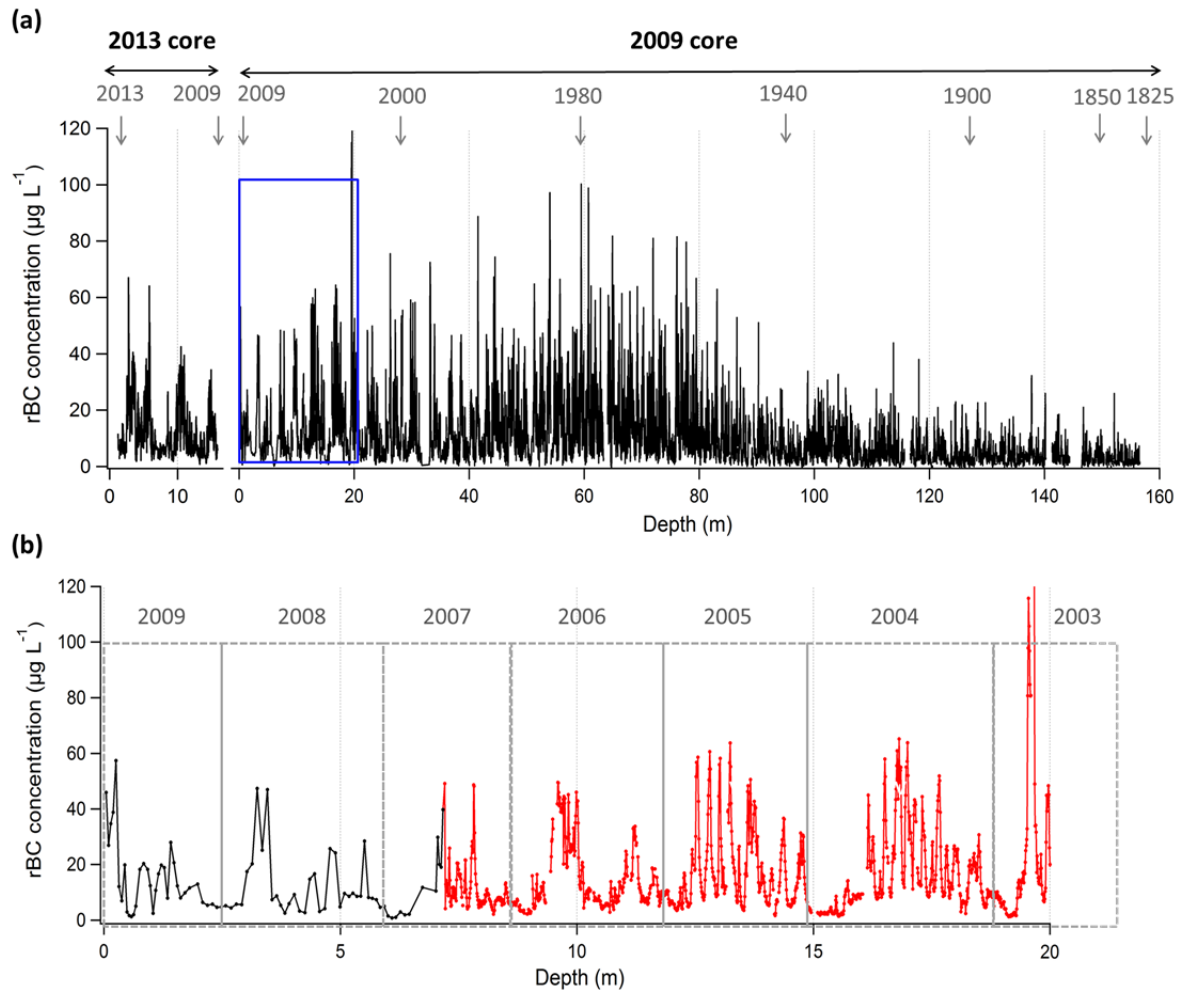
907
908    **Figure 3**
909
910
911
912
913
914
915
916
917
918
919
920
921
922
923
924
925

926 **(a)**
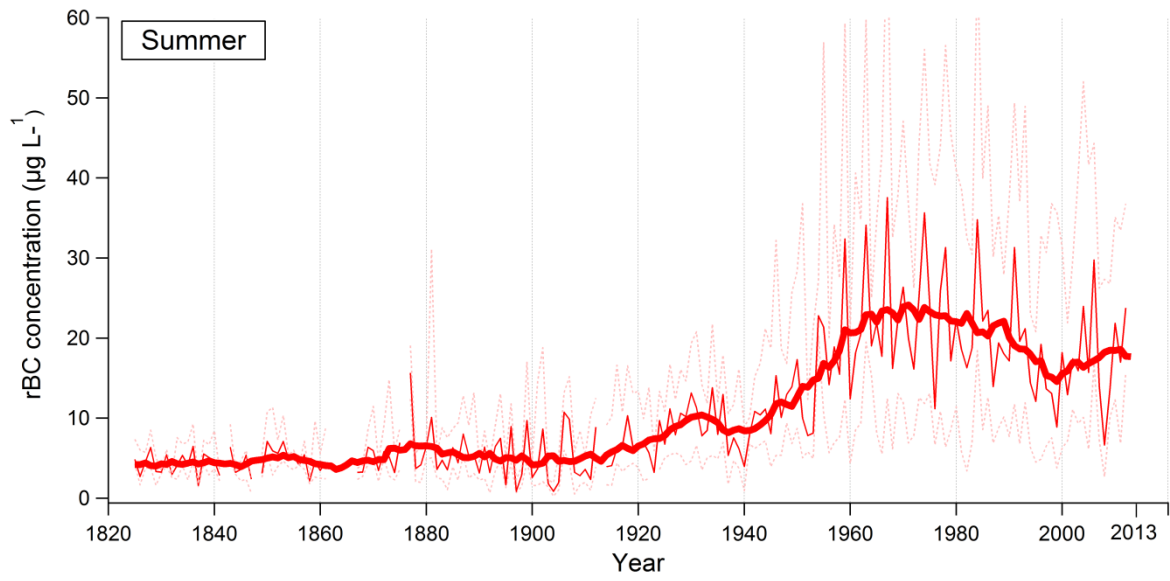


927
928
929 **(b)**



930
931
932 **(c)**

933
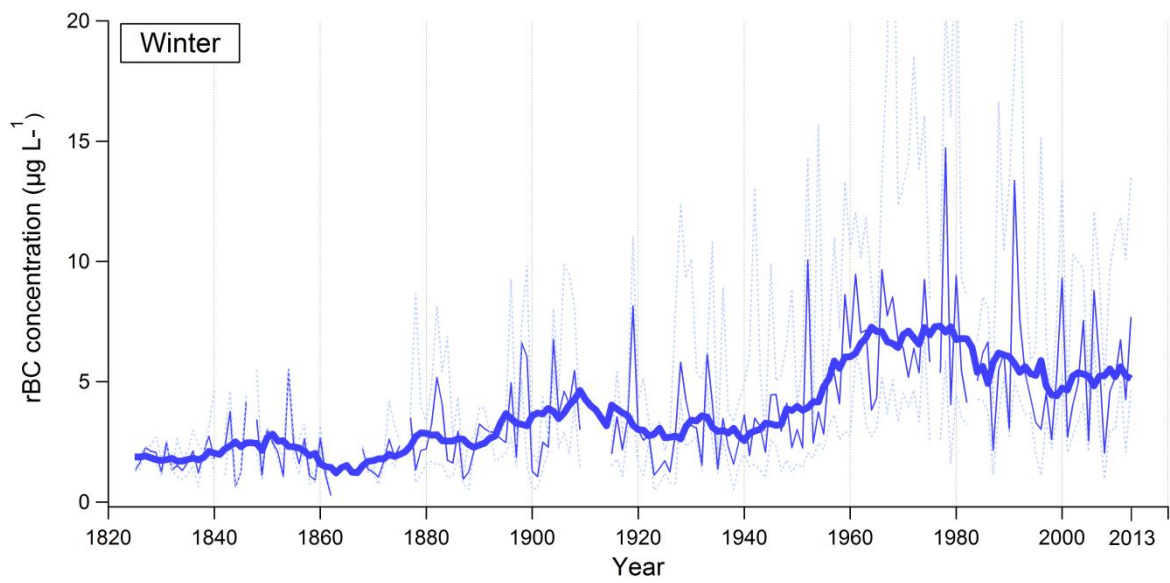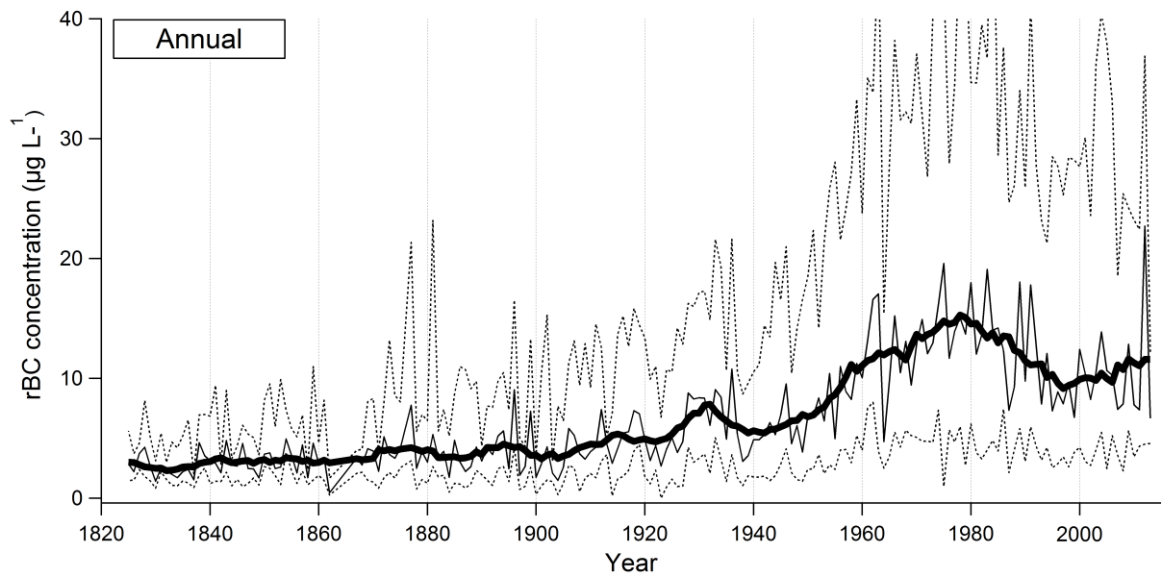
934 **Figure 4**

935

936



937
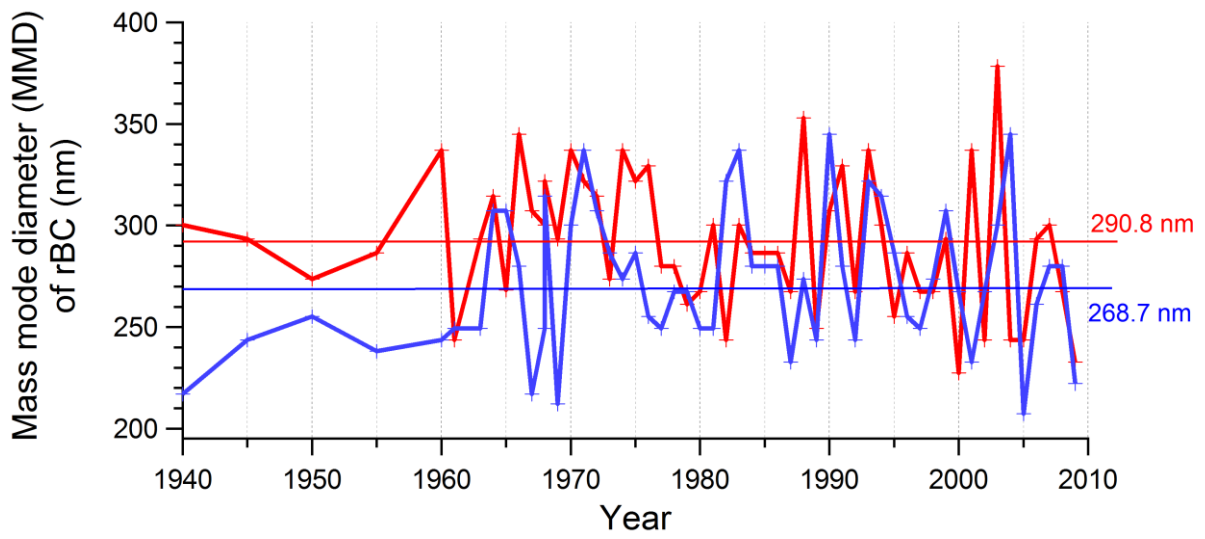
938 **Figure 5**

939

940

941

942

943

944

945

946

947
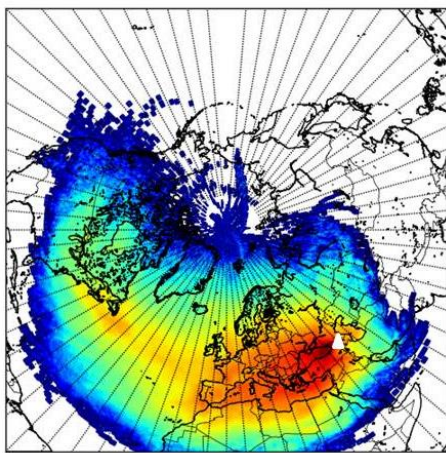
948 **(a)**                                    **(b)**
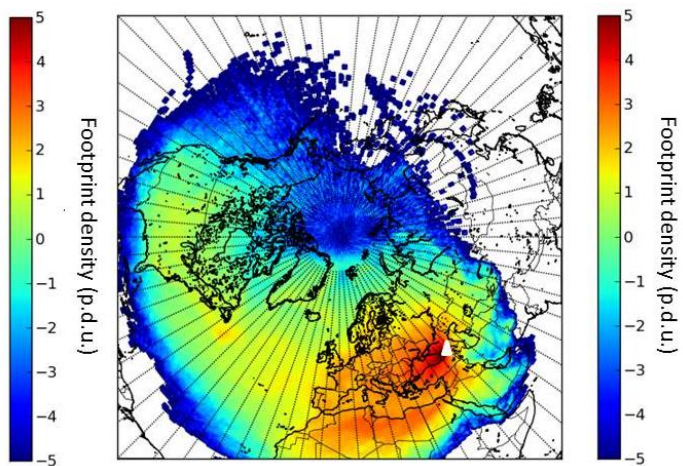


949

950 **(c)**
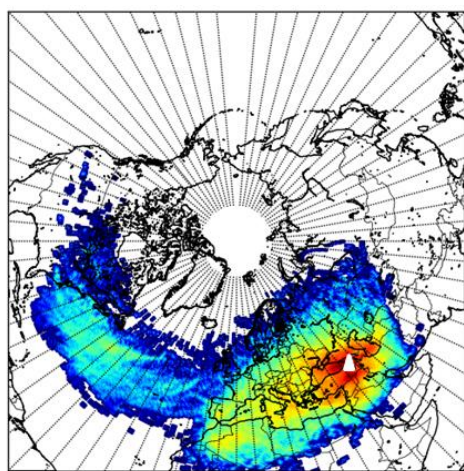


951

952 **Figure 6**

953

954

955

956

957

958

959

960

961

962

963

964

965

966

967    **(a)**
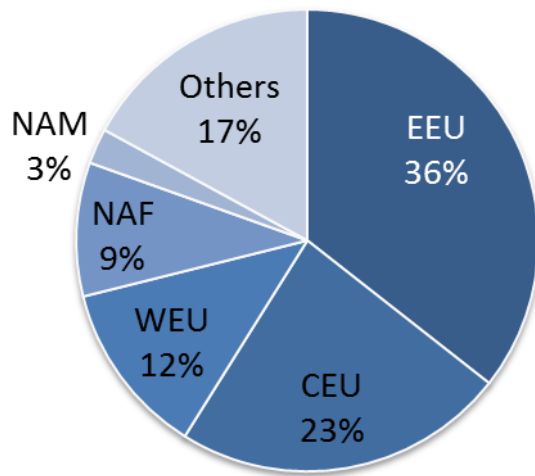


968    **(b)**
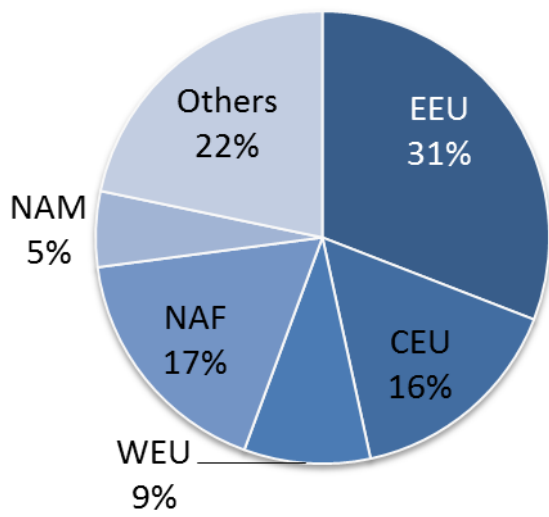


969

970 **(c)**
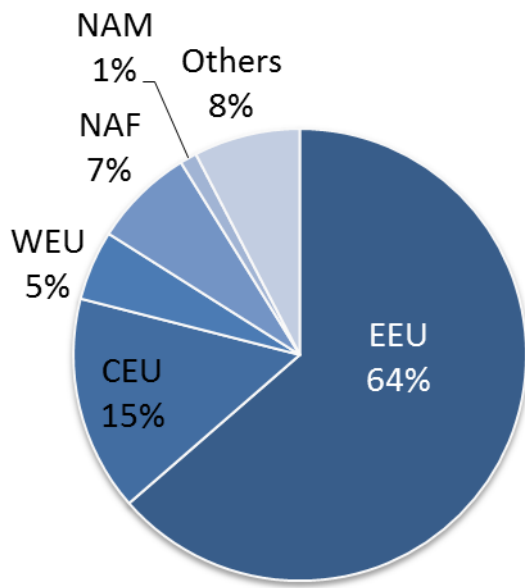


971
972 **Figure 7**
973
974
975
976
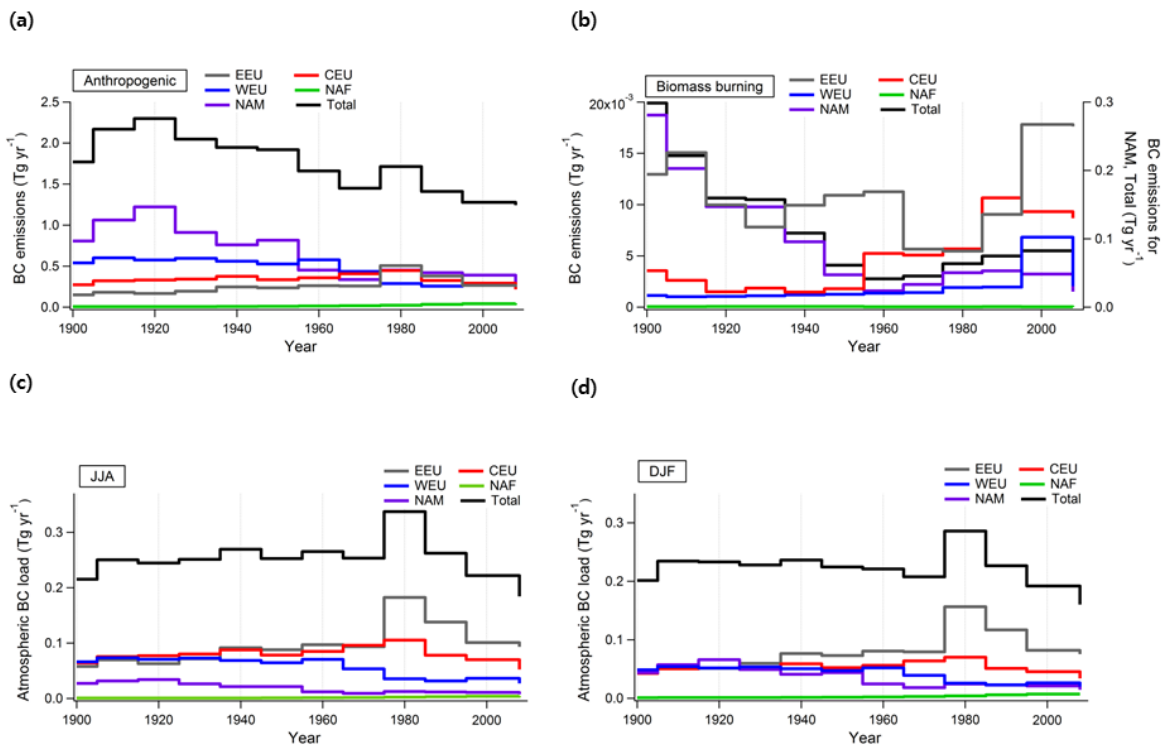


977
978 **Figure 8**
979
980

981     (a)
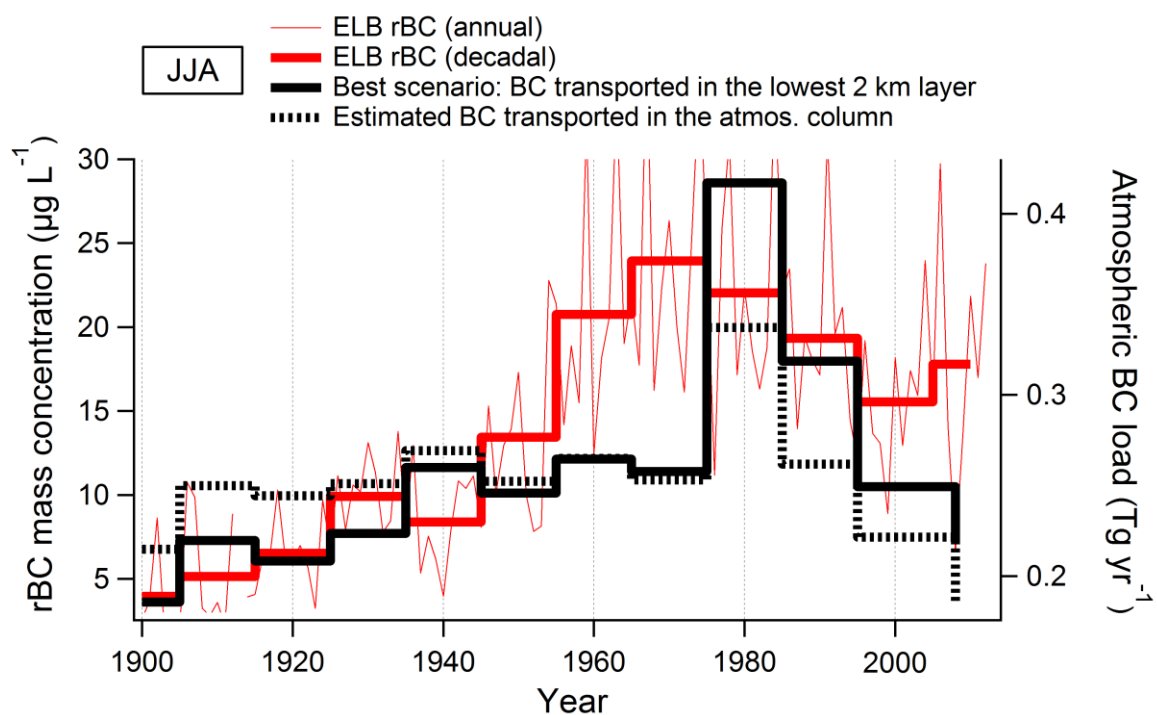


982
983     (b)
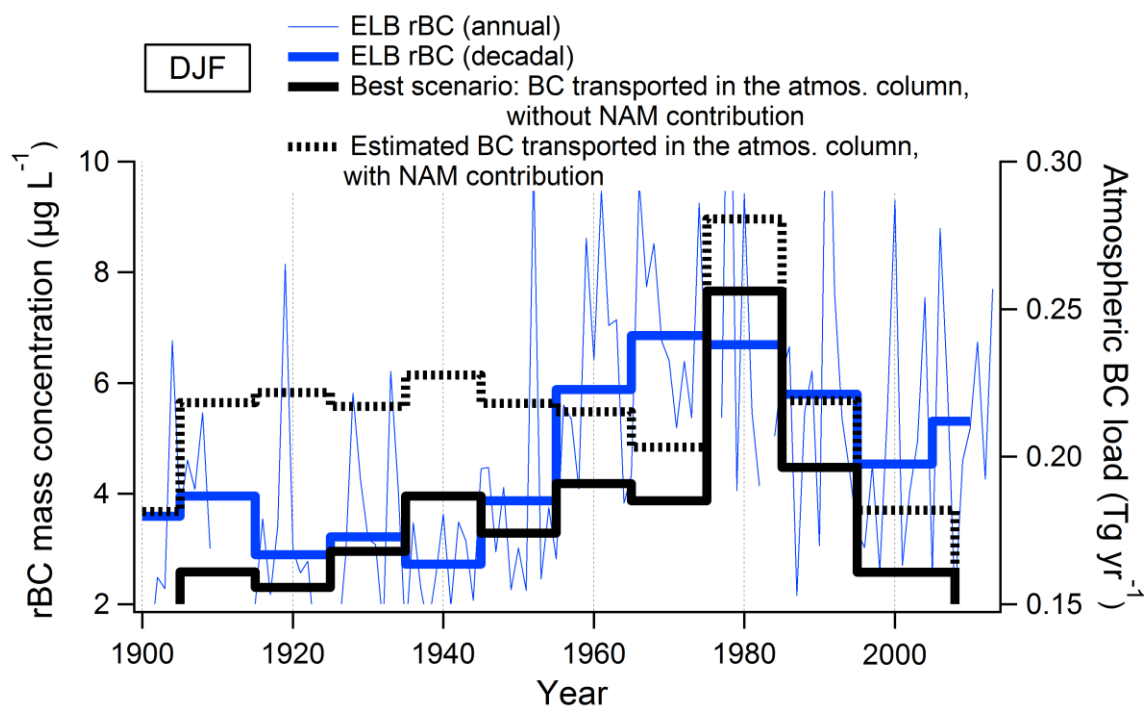


984
985     **Figure 9**
986
987
988
989
990